



UNIVERSITY OF LEEDS

This is a repository copy of *State parameter–based thermomechanical constitutive model for saturated fine-grained soils*.

White Rose Research Online URL for this paper:
<https://eprints.whiterose.ac.uk/177476/>

Version: Accepted Version

Article:

Zhu, Q-Y, Zhuang, P-Z, Yin, Z-Y et al. (1 more author) (2021) State parameter–based thermomechanical constitutive model for saturated fine-grained soils. *Canadian Geotechnical Journal*, 58 (7). pp. 1045-1058. ISSN 0008-3674

<https://doi.org/10.1139/cgj-2019-0322>

Reuse

Items deposited in White Rose Research Online are protected by copyright, with all rights reserved unless indicated otherwise. They may be downloaded and/or printed for private study, or other acts as permitted by national copyright laws. The publisher or other rights holders may allow further reproduction and re-use of the full text version. This is indicated by the licence information on the White Rose Research Online record for the item.

Takedown

If you consider content in White Rose Research Online to be in breach of UK law, please notify us by emailing eprints@whiterose.ac.uk including the URL of the record and the reason for the withdrawal request.



eprints@whiterose.ac.uk
<https://eprints.whiterose.ac.uk/>

State parameter–based thermomechanical constitutive model for saturated fine-grained soils

Qi-Yin Zhu, Pei-Zhi Zhuang, Zhen-Yu Yin, and Hai-Sui Yu

Fn1-Fn2

Abstract: This paper presents a two-surface constitutive model for describing thermomechanical behaviour of saturated fine-grained soils at both normally consolidated and overconsolidated states. A thermal-dependent stress ratio-state parameter relation is adopted to account for the effects of temperature on the shape of the state boundary surface (SBS) of soils. In the model, both the size and the shape of the SBS are allowed to vary with temperature, which is evidenced by thermal variation of the mechanical yield loci and the shifts of the normal consolidation line (NCL) and the critical state line (CSL) upon heating and (or) cooling. A thermal yield surface is added for modelling the isotropic thermal deformation of soils more accurately, in particular at overconsolidated states. The mechanical and thermal yield mechanisms are coupled through the temperature-dependent preconsolidation pressure that is controlled by a volumetric hardening law. Based on experimental observations, a nonlinear relationship between the spacing ratio and temperature changes is defined and a simple thermal dependent non-associated flow rule is proposed. The model is validated against some selected experimental results of several soils tested under various mechanical and thermal paths such as drained isotropic heating and cooling, drained and undrained triaxial compression at non-isothermal conditions.

Key words: temperature effects, constitutive relations, clays, plasticity, state parameter.

Résumé : Cet article présente un modèle constitutif à deux surfaces pour décrire le comportement thermomécanique des sols saturés à grains fins à l'état normalement consolidé et surconsolidé. Une relation entre le rapport de contrainte et les paramètres d'état dépendant de la température est adoptée pour tenir compte des effets de la température sur la forme de la surface limite d'état (SBS) des sols. Dans le modèle, tant la taille que la forme de la SBS peuvent varier avec la température, ce qui est mis en évidence par la variation thermique des lieux de rendement mécanique et les déplacements de la ligne de consolidation normale (NCL) et de la ligne d'état critique (CSL) lors du chauffage et/ou du refroidissement. Une surface de rendement thermique est ajoutée pour modéliser plus précisément la déformation thermique isotrope des sols, en particulier aux états surconsolidés. Les mécanismes de rendement mécanique et thermique sont couplés par la pression de préconsolidation dépendant de la température, qui est contrôlée par une loi de durcissement volumétrique. Sur la base d'observations expérimentales, une relation non linéaire entre le rapport d'espacement et les changements de température est définie et une simple règle d'écoulement non associée dépendant de la température est proposée. Le modèle est validé par rapport à certains résultats expérimentaux sélectionnés de plusieurs sols testés sous diverses voies mécaniques et thermiques telles que le chauffage et le refroidissement isotrope drainé, la compression triaxiale drainée et non drainée dans des conditions non isothermiques. [Traduit par la Rédaction]

Mots-clés : effets de la température, relations constitutives, argiles, plasticité, paramètre d'état.

Introduction

Significant temperature changes in soils may occur due to daily and seasonal temperature variations, heat transfer between geothermal structures and the surrounding soil (Bourne-Webb et al. 2016; Laloui and Di Donna 2013), heat release of nuclear waste disposal (Baldi et al. 1991; Graham et al. 1997), and energy dissipation during soil deformation (Pinyol et al. 2018). The thermomechanical behaviour of soils may greatly affect the stability of soil itself and the safety and performance of associated geostructures (e.g., pavement (Teltayev and Suppes 2019), energy piles, tunnels and

walls (Barla et al. 2016; Bourne-Webb et al. 2019; Di Donna et al. 2017; Laloui et al. 2006), buried pipes and cables (di Schio et al. 2016; Mitchell and Abdel-hadi 1979), petroleum drilling (Chen et al. 2003; Li et al. 2019)). Thus, understanding and modelling of the effects of temperature changes on the engineering properties of soils have been the subject of many studies in environmental geomechanics.

After the pioneering work by Campanella and Mitchell (1968), extensive experimental investigations on the thermomechanical behaviour of soils, particularly water-saturated clays, have been

Received 20 May 2019. Accepted 2 September 2020.

Q.-Y. Zhu. State Key Laboratory for Geomechanics and Deep Underground Engineering, China University of Mining & Technology, Xuzhou 221116, China.

P.-Z. Zhuang. School of Qilu Transportation, Shandong University, Jinan 250002, China.

Z.-Y. Yin. Department of Civil and Environmental Engineering, Hong Kong Polytechnic University, Hung Hom, Kowloon, Hong Kong, China.

H.-S. Yu. School of Civil Engineering, University of Leeds, Leeds LS2 9JT, UK.

Corresponding author: Pei-Zhi Zhuang (email: pzzhang@leeds.ac.uk).

Z.-Y. Yin served as an Editorial Board Member and handled manuscript review and acceptance; peer review and editorial decisions regarding this manuscript were handled by D. Sheng.

[†]Formerly School of Civil Engineering, University of Leeds, LS2 9JT Leeds, UK.

Copyright remains with the author(s) or their institution(s). Permission for reuse (free in most cases) can be obtained from copyright.com.

conducted (e.g., Abuel-Naga et al. 2007b; Baldi et al. 1991; Cekerevac and Laloui 2004; Ghahremannejad 2003; Hueckel and Baldi 1990; Kuntiwattanakul et al. 1995; Ng et al. 2019; Shetty et al. 2019; Sultan et al. 2002; Tanaka et al. 1997; Towhata et al. 1993; Uchaipichat and Khalili 2009). It was shown that temperature strongly affects the behaviour of fine-grained soils mainly through its influences on the soil structure and the free and absorbed water. Thorough discussions on the main thermomechanical behaviour of saturated clays from the perspective of constitutive modelling were made by Cui et al. (2000), Laloui and François (2009), and Mašin and Khalili (2012), among others. Here some important and general characteristics are summarized as follows:

- AQ1**
1. Temperature influences the normal consolidation line (NCL) of a soil; NCLs at different temperatures are approximately parallel to each other in the semi-logarithmic v - $\ln p$ plot (soil specific volume, v ; mean effective stress, p).
 2. Heating a saturated soil under drained conditions induces volume changes that strongly depends on the stress history (e.g., the overconsolidation ratio (OCR)).
 3. The size and the shape of the yield surface are temperature-dependent; thermal loadings could lead to either an increase or a decrease in the soil peak strength.

Based on experimental observations, various thermomechanical constitutive models were proposed over the past three decades taking some well-validated isothermal mechanical soil models as the basis. The basic framework for modern thermoplasticity constitutive modelling is largely attributed to the pioneering work by Hueckel and Borsetto (1990) and Hueckel and Baldi (1990). In recent years, constitutive studies based on other frameworks such as hypoplasticity theory (Mašin and Khalili 2012) and different thermodynamic approaches (Bai et al. 2019; Xiao 2014; Zhang and Cheng 2017) have also been carried out for describing the thermomechanical behaviour of soils. In this study, the more commonly known and widely used framework of Hueckel and Borsetto (1990) is followed. Before presenting the model, some relevant pioneering works in this general framework are reviewed as follows.

Hueckel and Borsetto (1990) extended the modified Cam-clay model by defining the size of the yield surface as a function of temperature as well as volumetric plastic strain. However, it has been found that the thermoplastic deformation at overconsolidated states cannot be well described. To tackle this issue, many subsequent models within the same framework were developed by introducing an additional thermal yield (TY) surface (Abuel-Naga et al. 2007a; Cui et al. 2000; Hong et al. 2016), the bounding surface concept (Laloui and Cekerevac 2003; Laloui and François 2009; Robinet et al. 1996; Zhou and Ng 2015), sub-loading surface theory (Yao and Zhou 2013), double hardening mechanism (Liu and Xing 2009), or approximate relationships between the thermally induced plastic strain and OCR (Graham et al. 2001). In addition, as the conventional Cam-clay type yield functions tend to significantly overestimate failure stresses on the "dry" side, the Hvorslev surface is often used at the overconsolidated states under both isothermal and non-isothermal conditions (Graham et al. 2001; Yao and Zhou 2013). Many important aspects of the thermomechanical behaviour of saturated clays can be satisfactorily described by these models, and an interesting comparison between some of them was recently provided by Hong et al. (2013).

In addition to the thermal evolutions of the size of the yield surface that was widely studied, some experimental evidence (e.g., Abuel-Naga et al. (2009), Cekerevac and Laloui (2004), Ghahremannejad (2003), Kuntiwattanakul et al. (1995)) showed that the shape of the yield surface may also vary with temperature. To account for the thermal variation of the shape of the state boundary surface (SBS), Hueckel et al. (2009) assumed the critical state friction angle of soil to be thermal dependent. However, this is not consistent with the

majority of existing test data (Cekerevac and Laloui 2004; Hong et al. 2016; Hueckel and Baldi 1990; Mašin and Khalili 2012; Tanaka et al. 1997). While regarding that the slope of the critical state line (CSL) in the p - q space (i.e., M ; deviatoric stress, q) is independent of temperature, the thermal dependency of the shape of SBSs cannot be described by those models relying on the conventional Cam-clay yield functions in the framework of Hueckel and Borsetto (1990). To overcome this limitation, several approaches were attempted in recent years. Abuel-Naga et al. (2009) introduced a temperature-related fabric parameter into the modified Camclay model, which allows the shape of the SBS to vary with temperature. This model was developed for characterizing the thermomechanical behaviour of normally consolidated and slightly overconsolidated clays (i.e., on the "wet" side). Focusing on the isothermal behaviour of saturated clays, Hamidi and Khazaei (2010) and Hamidi et al. (2015) modified the Cam-clay type flow rule with inclusions of temperature effects, and thermal shape flexibility was therefore introduced in the back-integrated yield surfaces. Zhou and Ng (2015) assumed linear variations of the vertical positions of the NCL and the CSL in the v - $\ln p$ space with changes of temperature, respectively. As a result, the shape of the SBS varies with temperature due to the thermal variation of the spacing ratio, adopting the clay and sand model (CASM) yield function proposed by Yu (1995) and Yu (1998). As a thermal-independent flow rule was adopted, the observed effect of temperature on the plastic flow (e.g., Abuel-Naga et al. (2009), Cekerevac and Laloui (2004), Hamidi et al. (2015), Uchaipichat and Khalili (2009)) cannot be fully captured by this model.

This paper aims to present an elastoplastic constitutive model for describing the short-term thermomechanical behaviour of both normally consolidated and overconsolidated saturated fine-grain soils under non-isothermal conditions. Two yield surfaces are introduced and coupled in the new model. Specifically, the mechanical yield (MY) surface is defined by extending the isothermal model of CASM with consideration of the temperature effects and the TY surface is added to describe the thermally induced deformation more realistically, particularly at overconsolidated states. Within the considered temperature range (without freezing or boiling of the pore water), the novelty and usefulness of the new model mainly lie in three aspects:

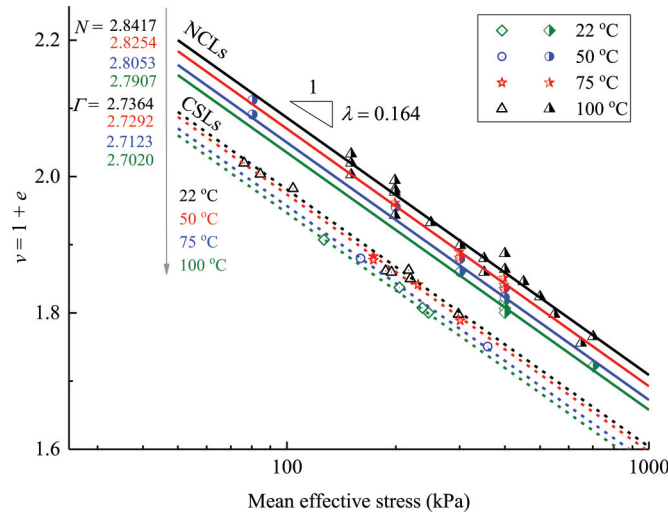
- AQ2**
1. Both the size and the shape of the MY surface are allowed to vary with temperature. The change in the size is controlled by the preconsolidation pressure that evolves with both thermal and mechanical volumetric plastic strains obeying a newly defined coupling mechanism; the shape variability depends on the thermal dependency of the spacing ratio, owing to the non-equal shifts of the NCLs and the CSLs when the soil is heated. A nonlinear thermal evolution law for the spacing ratio is defined based on available test observations.
 2. The mechanical behaviour of both normally consolidated and overconsolidated soils at elevated temperatures can be accurately described for both drained and undrained conditions, partly inherited from the mother model of CASM. **A new thermal dependent non-associated flow rule is proposed and used.**

Finally, the proposed model is validated against experimental results of selected element tests in the literature, which include several fine-grained soils and various thermal, stress or combined loading paths such as drained isotropic heating-cooling, drained and undrained triaxial compression tests at elevated temperatures.

State boundary surface (SBS)

SBS is defined as a boundary of all possible states of a soil element in the p - q - v space (Schofield and Wroth 1968). The NCL represents a

Fig. 1. Measured and fitted normal consolidation lines (NCLs) and critical state lines (CSLs) for M44 clay at different temperatures (modified after Ghahremannejad 2003). [Colour online.]



trace of the SBS in the $p-v$ plane, and the yield loci represent its projection in the deviatoric stress plane (i.e., $p-q$ plane). Constitutive equations can be established by relating the SBS to a family of yield loci in an equivalent two-dimensional stress plane. For example, in Cam-clay models (Roscoe and Burland 1968; Roscoe et al. 1958), the yield surfaces in the $p-q$ plane are normalized by the preconsolidation pressure that is assumed to evolve with plastic volumetric strains based on the uniqueness of the normalized SBS of isotropically consolidated reconstituted soils at room temperature.

Under non-isothermal conditions, a number of experimental data showed that the NCL moves downwards at elevated temperatures (namely, lower specific volumes at higher temperatures) due to the thermal compaction and NCLs at different temperatures are almost parallel to each other (Abuel-Naga et al. 2007b; Burghignoli et al. 1992; Campanella and Mitchell 1968; Laloui and Di Donna 2013). Similar downward shifts of the CSLs were observed (Cekerevac and Laloui 2004; Graham et al. 2001). Meanwhile, although exception was reported (Cekerevac and Laloui 2004), a majority of experimental data showed that the NCL may remain parallel to the CSL for reconstituted soils at different temperatures (e.g., Fig. 1) (Ghahremannejad 2003; Graham et al. 2001; Lingnau et al. 1995; Tanaka 1995), and this was commonly accepted as a fundamental hypothesis in many thermo-mechanical soil models based on the critical state concept (e.g., Cui et al. (2000), Graham et al. (2001), Hueckel and Borsetto (1990), Seneviratne et al. (1993), Zhou and Ng (2015)).

Based on the aforementioned findings, the effects of temperature on the preconsolidation pressure ($p_{c(T)}$) and the corresponding critical state stress ($p_{s(T)}$) are illustrated in Fig. 2. These two representative pressures are often correlated by the spacing ratio of NCL and CSL, that is $r_{(T)} = p_{c(T)}/p_{s(T)}$ (Wroth 1984). At a constant plastic strain condition (i.e., on the same swelling line), $p_{c(T)}$ and $p_{s(T)}$ become smaller at higher temperatures as the NCL and CSL shift downwards in the $v-p$ plane, respectively. As a result, the SBS shrinks when the soil is heated (Mašin and Khalili 2012). Thermal evolutions of the NCL and the CSL are not necessarily always the same (Cekerevac and Laloui 2004; Ghahremannejad 2003; Kuntiwattanakul et al. 1995; Tanaka et al. 1997; Uchaipichat and Khalili 2009), which thus leads the spacing ratio to be temperature dependent.

In standard Cam-clay models, the same spacing ratio values are used for all soil types (namely, 2.718 and 2 for the original and the

modified Cam-clay models, respectively (Wroth 1984; Yu 1998) although in reality this is not always the case. In particular, while the standard Cam-clay yield curves (normalized by $p_{c(T)}$) are used directly in non-isothermal conditions, the aforementioned temperature dependency of the spacing ratio cannot be accounted for. Instead, it is very convenient to introduce the general stress-state relationship proposed by Yu (1998), namely:

$$(1) \quad \left(\frac{\eta}{M}\right)^n = 1 - \frac{\xi_{(T)}}{\xi_{R(T)}}$$

where η is the stress ratio ($= q/p$); n is a material constant, which controls the curvature of the yield surface and typically ranges between 1.0–5.0; $\xi_{(T)}$ represents “the state parameter” (Been and Jefferies 1985; Yu 1998); $\xi_{R(T)}$ is a reference parameter, which represents the vertical distance between the NCL and the CSL at a given temperature and equals $(\lambda - \kappa) \ln r_{(T)}$ (Fig. 2).

$$(2) \quad \xi_{(T)} = v + \lambda \ln p - \Gamma_{(T)}$$

where $v = 1 + e$, and e is the void ratio; $\Gamma_{(T)}$ denotes the specific volume of the temperature-dependent CSL at $p = 1$ kPa; λ and κ are the slopes of the NCL (or CSL) and the swelling line in the $v-\ln p$ space (see Fig. 2), respectively.

For fine-grained soils, the overconsolidation ratio ($\text{OCR} = p_{c(T)}/p$) is more often used to define the soil state. As depicted in Fig. 2, eq. 2 can be equivalently expressed as:

$$(3) \quad \xi_{(T)} = (\lambda - \kappa) \ln \left(\frac{r_{(T)}}{\text{OCR}} \right)$$

It is important to note that $\text{OCR} = r_{(T)}$ (or $\xi_{(T)} = 0$) at the critical state; $\text{OCR} < r_{(T)}$ on the “wet” side (i.e., soft clay, $\xi_{(T)} > 0$); $\text{OCR} > r_{(T)}$ on the “dry” side (i.e., stiff clay, $\xi_{(T)} < 0$).

It is clear that in eq. 1 the spacing ratio is allowed to vary with material type and temperature. In other words, the SBS is generalized to accommodate the complex thermal-dependent behaviour of various soils, providing a link between classical critical state soil mechanics and thermomechanical constitutive modelling. By normalizing eq. 1 with the preconsolidation pressure, a generalized yield surface in the $p-q$ plane is obtained as:

$$(4) \quad f^{\text{MY}} = \left(\frac{q}{Mp}\right)^n + \frac{\ln(p/p_{c(T)})}{\ln r_{(T)}}$$

The yield function of the original Cam-clay model can be recovered exactly by choosing $n = 1$ and $r_{(T)} = 2.718$, and the “wet” side of the modified Cam-clay model can be matched accurately by choosing $r_{(T)} = 2$ in conjunction with a suitable value of n (typically around 1.5–2) in eq. 4. In agreement of the majority of the published experimental data (e.g., Cekerevac and Laloui (2004), Hong et al. (2016), Hueckel and Baldi (1990), Tanaka et al. (1997)), M is assumed to be temperature independent in the present model. The material constant n is also assumed to be independent of temperature. In eq. 4, thermal variations of the SBS (size and shape) are controlled by thermal evolutions of the preconsolidation pressure (i.e., $p_{c(T)}$) and the spacing ratio (i.e., $r_{(T)}$), and they will be defined in the next section. It needs to be pointed out that conflict results with regard to the dependencies of M and n on the temperature were reported for some particular soils (Hamidi et al. 2015; Hueckel and Pellegrini 1991). However, this is not taken into account in the present basic model due to the lack of compelling evidence.

Thermoelastoplastic modelling

Assuming compressive stress and strain as positive, two stress variables normally used in critical state soil mechanics are defined as:

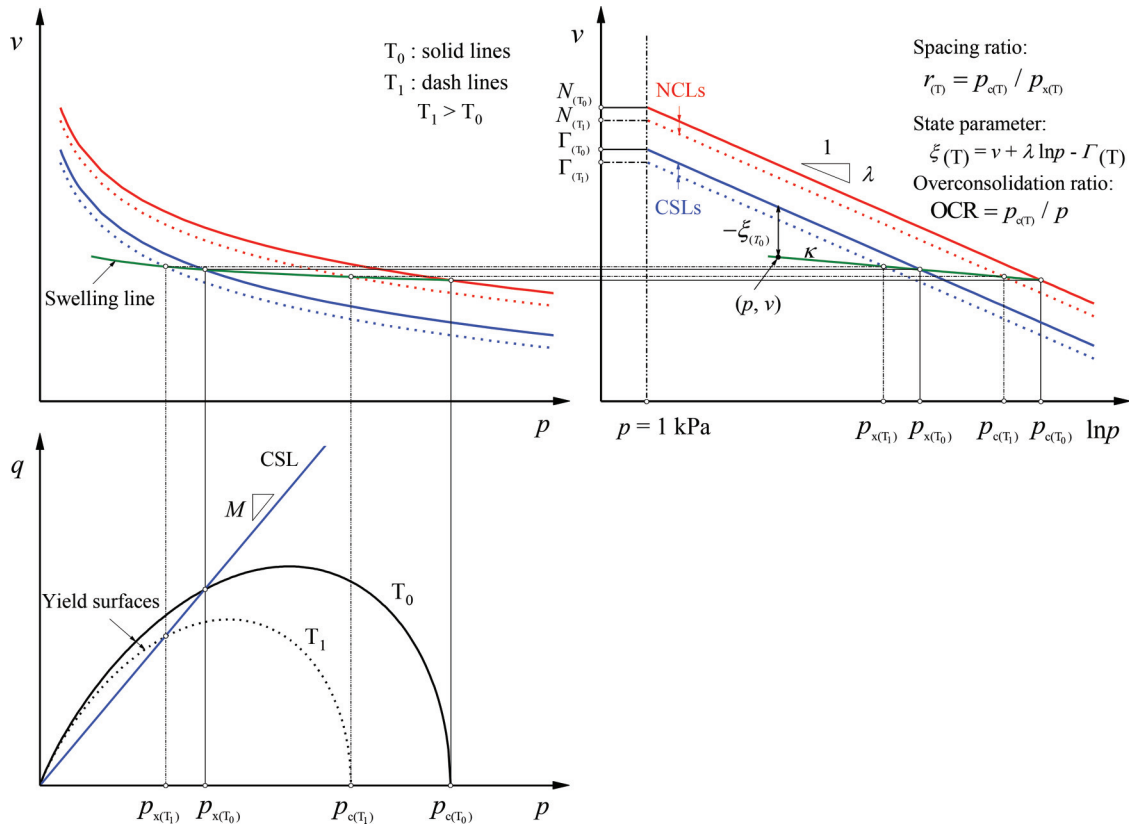
AQ3

AQ4

F1

F2

Fig. 2. Definitions and example relationships among NCLs, CSLs, and yield loci. [Colour online.]



$$(5a) \quad p = \sigma_{ii}/3 = (\sigma_{11} + \sigma_{22} + \sigma_{33})/3$$

$$(5b) \quad q = \sqrt{3(\sigma_{ij} - p\delta_{ij})\sigma_{ij} - p\delta_{ij}/2}$$

where σ_{ij} is the principal effective stress tensor; δ_{ij} is the Kronecker delta. For notation convenience, all stress variables in this paper are effective values.

The volumetric and deviatoric strain increments are defined as:

$$(6a) \quad d\varepsilon_v = d\varepsilon_{11} + d\varepsilon_{22} + d\varepsilon_{33}$$

$$(6b) \quad d\varepsilon_d = \frac{2}{3} \sqrt{(d\varepsilon_{11} - d\varepsilon_{22})^2 + (d\varepsilon_{11} - d\varepsilon_{33})^2 + (d\varepsilon_{33} - d\varepsilon_{22})^2}$$

where ε_v and ε_d denote the volumetric and deviatoric strains, respectively; ε_{ii} are principal strain components. The total strain increments are split into elastic and plastic components (i.e., $d\varepsilon_v = d\varepsilon_v^e + d\varepsilon_v^p$ and $d\varepsilon_d = d\varepsilon_d^e + d\varepsilon_d^p$), which depend on both mechanical and thermal loadings. They are treated separately in the small deformation domain as shown subsequently. Note that heating and (or) cooling of the soil are assumed to be under drained conditions in this paper.

Elastic behaviour

For elastic deformation, it is common to assume that temperature changes only induce elastic volumetric strain in soils (Abuel-Naga et al. 2007a; Cui et al. 2000; Hueckel and Borsetto 1990; Laloui and François 2009; Yao and Zhou 2013). In other words, the elastic deviatoric strain is solely associated with mechanical loading. As a result, the thermoelastic strain increments can be defined as:

$$(7) \quad d\varepsilon_v^e = \frac{\kappa}{1+e} \frac{dp}{p} - \alpha dT$$

$$(8) \quad d\varepsilon_d^e = \frac{2(1+\mu)}{9(1-2\mu)} \frac{\kappa}{1+e} \frac{dq}{p}$$

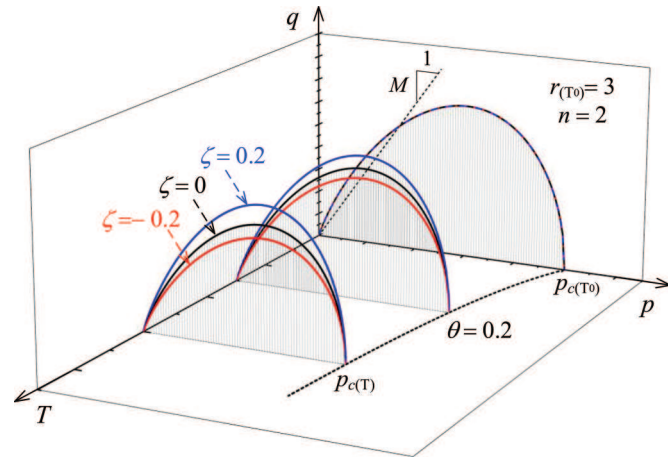
where α is the drained elastic volumetric thermal expansion coefficient; μ is Poisson's ratio, and it is assumed to be constant for a given soil. It was shown that α may essentially be considered as independent of stress state and temperature (Cui et al. 2000; Hong et al. 2013; Mašin and Khalili 2012; Sultan et al. 2002). Therefore, a constant value of α is assumed in the eq. 7.

In eqs. 7 and 8, the mechanically induced strains are described by using the hypoelastic model as in Cam-clay models (Wood 1990). Although thermal dependent κ has been reported (Eriksson 1989; Graham et al. 2001), many results showed that the slope of the swelling line (κ) is temperature independent (Abuel-Naga et al. 2007b; Campanella and Mitchell 1968; Cui et al. 2000). It was argued by Abuel-Naga et al. (2007b) that this discrepancy is due to the difference in the test procedure, and a constant value of κ is preferable for defining the mechanical elastic behaviour within the yield limit. This is adopted in the present model. It needs to be pointed out that thermal variations of κ , if any, would lead to additional changes to the critical state stress than purely caused by the thermal shift of the CSL, and thereby could further alter the shape of the SBS (Tanaka 1995).

Thermomechanical yield curves

In the framework of elastic–plastic theory, thermomechanical yield curves describe the boundary of a thermoelastic domain, within which reversible deformation occurs due to changes of temperature or effective stresses or both. In this model, similar to Cui et al. (2000) and Abuel-Naga et al. (2007a), two yield

Fig. 3. Size and shape variation with temperature increase at constant plastic strain. [Colour online.]



surfaces are introduced in the p - T plane, namely MY surface and TY surface. The former corresponds to the thermal evolution of the SBS in the p - q space, and the latter mechanism is for describing the thermally induced volume change of soil more realistically.

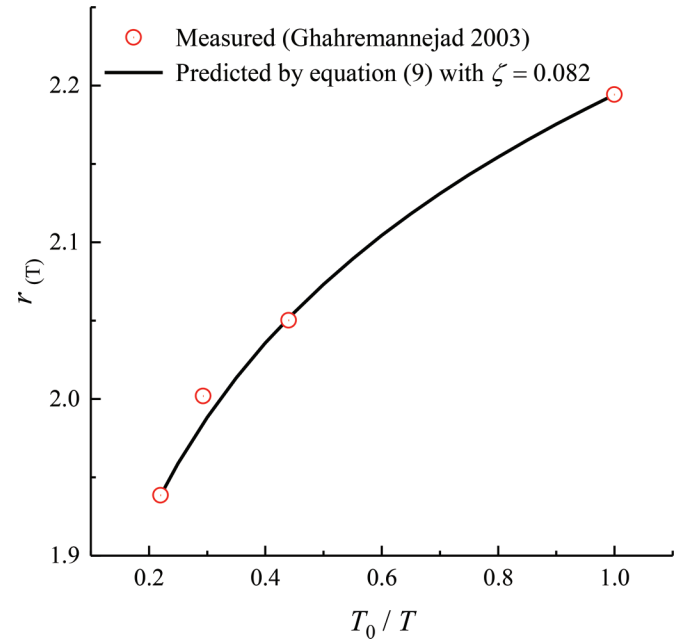
Mechanical yield (MY) limit

The MY surface in the p - q space was defined in eq. 4. Subjected to temperature changes, the size of the SBS varies due to the thermal evolution of the preconsolidation pressure (i.e., $p_{c(T)}$) (Cui et al. 2000; Hueckel and Borsetto 1990; Laloui and Cekerevac 2003; Wang et al. 2016). Several evolution laws of $p_{c(T)}$ in response to temperature changes at constant plastic strain (i.e., at no heat-induced plastic strain) were proposed in the p - T plane (Hueckel and Borsetto 1990; Laloui and Cekerevac 2003; Moritz 1995). Based on available experimental data of a variety of soils, Moritz (1995) and Wang et al. (2016) demonstrated that it is reasonable to assume a linear relationship between $\ln[p_{c(T)}/p_{c(T_0)}]$ and $\ln(T/T_0)$, that is

$$(9) \quad \ln \left[\frac{p_{c(T)}}{p_{c(T_0)}} \right] = \theta \ln \left(\frac{T_0}{T} \right)$$

where $p_{c(T_0)}$ is the preconsolidation pressure at reference (or room) temperature T_0 ; θ is a material parameter that determines the thermal dependence of the preconsolidation pressure. With a positive value of θ , eq. 9 predicts a nonlinear decrease of $p_{c(T)}$ with temperature increases (e.g., Fig. 3). Wang et al. (2016) validated this relationship with seven types of clays and also pointed out that eq. 9 in fact is the first-order approximation of the dependency law of Laloui and Cekerevac (2003). Meanwhile, the shape of the SBS may also change with temperature (Abuel-Naga et al. 2009; Hamidi et al. 2015; Hong et al. 2016; Hueckel et al. 2009; Mašin and Khalili 2012; Zhou and Ng 2015). This thermal variation may be attributed to the thermally induced irreversible changes of soil structure (fabric) (Abuel-Naga et al. 2009; Zymnis et al. 2018), and it can be captured by allowing the spacing ratio (i.e., $r_{(T)}$) in the yield function to be temperature dependent. As shown in Fig. 2, $\ln[p_{c(T)}/p_{c(T_0)}]$ is the horizontal distance between the NCLs at T_0 and elevated temperature T , respectively, at a constant plastic strain condition. It is assumed that the translation of the CSL due to temperature changes is similar to that of the NCL. Therefore, by definition, the thermal variation of the spacing ratio can be expressed as:

Fig. 4. Measured and predicted thermal variation of spacing ratio for M44 clay. [Colour online.]



$$(10) \quad \ln \left[\frac{r_{(T)}}{r_{(T_0)}} \right] = \zeta \ln \left(\frac{T_0}{T} \right)$$

where $r_{(T_0)}$ denotes the spacing ratio at the reference temperature T_0 ; ζ is a constant value that controls the thermal variation of the spacing ratio. The influence of the thermal evolution of $r_{(T)}$ on the yield surface is illustrated in Fig. 3. According to eqs. 9 and 10, the horizontal translation of the CSL due to the temperature change of $(T - T_0)$ (i.e., $\ln[p_{c(T)}/p_{c(T_0)}]$) equals $(\theta - \zeta) \ln(T_0/T)$. As the CSL may stay or move downwards in the v - $\ln p$ space when the soil is heated (Abuel-Naga et al. 2007b; Cekerevac and Laloui 2004; Ghahremannejad 2003; Kuntiwattanukul et al. 1995; Tanaka et al. 1997), $\zeta \leq \theta$ and ζ could be positive, zero or negative, which indicates that the parallel shift of the CSL is smaller, the same or greater, respectively, than that of the NCL with the same temperature change. For example, compared to the experimental data of Ghahremannejad (2003) (refer to Fig. 1), Fig. 4 shows that eq. 10 with $\zeta = 0.082$ agrees well with the measured results; on the contrary, a negative value of ζ was calibrated from results of drained triaxial tests on Bourke silt at different temperatures that were performed by Uchaipichat and Khalili (2009) (see Table 1) as detailed subsequently.

Thermal yield (TY) limit

Upon drained heating, the volume change of soil greatly depends on the stress history (e.g., OCR). For example, with rising temperature, thermal contraction dominates at low values of OCR; whereas, the soil may dilate first and then transit to contract at intermediate OCRs. The transition temperature from expansion to contraction increases with higher OCR values (Abuel-Naga et al. 2007a; Baldi et al. 1988; Cekerevac and Laloui 2004; Cui et al. 2000; Sultan et al. 2002; Towhata et al. 1993). At very high OCRs, the soil may only experience thermal expansion in the temperature range without freezing or boiling of the pore water. Based on elastoplastic theory, the reversible thermal expansion is attributed to thermoelastic deformation (e.g., eq. 7), and the thermal contraction is interpreted as thermoplastic (Hueckel and Baldi 1990). It was reported that the transition

F3

F4

T1

Table 1. Summary of model parameters.

	Boom clay (Baldi et al. 1991)	Bangkok clay (Abuel-Naga et al. 2007b)	Illite clay (Tanaka 1995)	Bourke silt (Uchaipichat and Khalili 2009)
Isothermal parameters				
λ	0.12	0.59	0.087	0.09
κ	0.046	0.1	0.017	0.006
$p_{c(T_0)}$ *	2 MPa	200 kPa	1.5 or 1.0 MPa	200 kPa
M	—	—	1.07	1.25
n	—	—	1.3	2.5
$r_{(T_0)}$	—	—	2.05	2.1
μ	0.3	0.3	0.3	0.3
Temperature-related parameters				
α ($10^{-5}/^\circ\text{C}$)	5	6	6	8
θ	0.24	0.2	0.1	0.13
ζ	—	0.2	0.08	-0.12
β_0	3	6	5	6
ω ($10^{-5}/^\circ\text{C}^2$)	1.2	2.4	0.6	0.27

*Values of $p_{c(T_0)}$ are given here for convenience, by which the model parameter $\Gamma_{(T_0)}$ can be readily determined by using $\Gamma_{(T_0)} = v + \kappa \ln p + (\lambda - \kappa) \ln [p_{c(T_0)}/r_{(T_0)}]$.

temperature for overconsolidated soils is generally much lower than the yield limit predicted by the MY curve even though the thermal evolution of the preconsolidation pressure is considered (Abuel-Naga et al. 2007a; Coccia and McCartney 2016). Cui et al. (2000) proposed that this phenomenon can be captured by introducing a second yield curve (i.e., TY) in the p - T plane. Here, the TY curve proposed by Abuel-Naga et al. (2007a) (i.e., eq. 11) is followed.

$$(11) \quad \frac{p_{c(T_0)}}{p_{T(T)}} = \beta \sqrt{\ln \frac{T}{T_0}} + 1$$

Then the TY function can be written as

$$(12) \quad f^{TY} = p_{T(T)} \left(\beta \sqrt{\ln \frac{T}{T_0}} + 1 \right) - p_{c(T_0)} = 0$$

where $p_{T(T)}$ is the effective stress at the aforementioned transition temperature; β is the evolution parameter depending on the loading history, and its initial value is β_0 . Figure 5 shows example results calculated by eq. 11 with different fixed values of β in the p - T plane, under stresses below which the deformation is assumed to be thermoelastic. The adopted TY curve coincides with the MY curve at room temperature, which is in agreement with experimental observations (Abuel-Naga et al. 2007a).

Thermomechanical plastic strains

Mechanical plastic volumetric strain (ϵ_v^{mp}) is produced when the MY limit is reached. Following the conventional soil plasticity theory, mechanical plastic strain increments can be expressed as

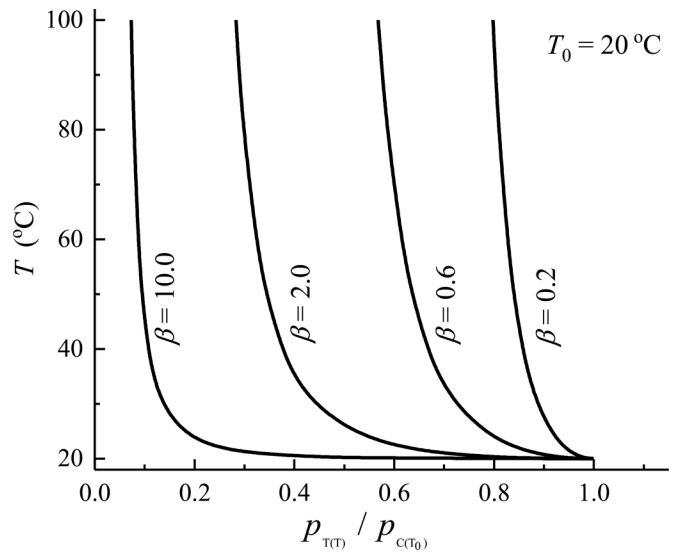
$$(13a) \quad d\epsilon_v^{mp} = d\lambda_m \frac{\partial g^{MY}}{\partial p}$$

$$(13b) \quad d\epsilon_d^{mp} = d\lambda_m \frac{\partial g^{MY}}{\partial q}$$

where $d\lambda_m$ is the plastic multiplier, a positive scalar; g^{MY} is the plastic potential function corresponding to mechanical loading; ϵ_d^{mp} is the plastic deviatoric strain due to mechanical loading, and $\epsilon_d^p = \epsilon_d^{mp}$ as no plastic deviatoric strain is induced by thermal loading.

Although the conventional Cam-clay type flow rules were often used directly at elevated temperatures (Cui et al. 2000; Graham et al. 2001; Laloui and François 2009; Zhou and Ng 2015), it was

Fig. 5. Example results of thermal yield (TY) limits.



shown that changes of the temperature may also affect the plastic flow rule (Abuel-Naga et al. 2007b; Hamidi et al. 2015). Hence, a simple thermal dependent flow rule is proposed in eq. 14 by slightly modifying the conventional Cam-clay type flow rule (Hong et al. 2016, 2020; McDowell and Hau 2003). Inspired by some experimental observations (Abuel-Naga et al. 2009; Hamidi et al. 2015; Uchaipichat and Khalili 2009), $k = 2 \ln r_{(T)}$ is assumed by simplifying the general stress-dilatancy relation proposed by Yu (2006).

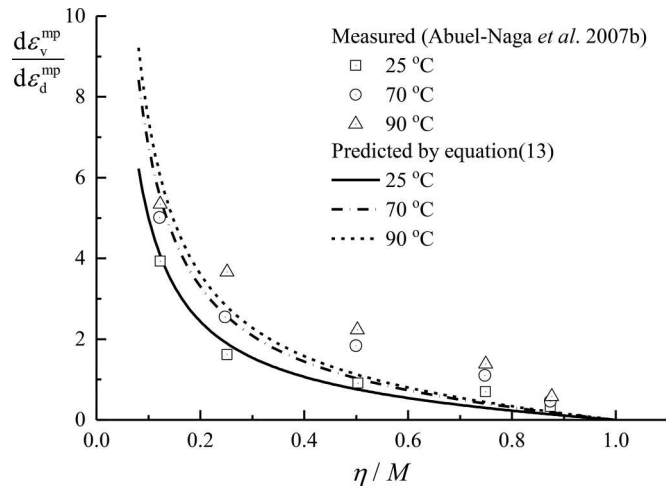
$$(14) \quad \frac{d\epsilon_v^{mp}}{d\epsilon_d^{mp}} = \frac{M^2 - \eta^2}{k\eta}$$

Then the non-associate plastic potential function g^{MY} can be readily obtained by integrating eq. 14 (Yu 2006) as:

$$(15) \quad g^{MY} = k \ln \left[1 + (k-1) \left(\frac{\eta}{M} \right)^2 \right] + 2(k-1) \ln \left(\frac{p}{C} \right)$$

where C indicates the size of the plastic potential surface, which can be determined by solving the preceding equation for any given stress state. It is noted that the potential function with $k = 2$ corresponds to the modified Cam-clay model.

Fig. 6. Measured and predicted stress–dilatancy relationships for soft Bangkok clay.



In eq. 14, the flow rule is related to the temperature-dependent spacing ratio. While ζ is positive, zero, or negative, the incremental plastic strain ratio (i.e., $d\varepsilon_v^{mp}/d\varepsilon_d^{mp}$) increases (Abuel-Naga et al. 2007b), remains unchanged (Graham et al. 2001), or decreases (Uchaipichat and Khalili 2009) with temperature increases, which coincides with experimental observations in the literature. For example, in soft Bangkok clay, Abuel-Naga et al. (2007b) observed that the NCLs move downwards while the CSLs almost remain unaltered when the soil is heated. Therefore, ζ is positive and close to the value of θ (e.g., Table 1). With a positive value of ζ , eq. 14 predicts that $d\varepsilon_v^{mp}/d\varepsilon_d^{mp}$ increases as temperature rises, and this is consistent with the experimental observation (Fig. 6). Note that underestimation of the temperature effect is shown at high stress ratios. This can be alleviated by including several additional model parameters (Hamidi et al. 2015). However, this was not attempted in this study to keep the model consistent and simple.

Then, the plastic multiplier $d\lambda_m$ can be determined from the consistency condition of the MY function, as follows:

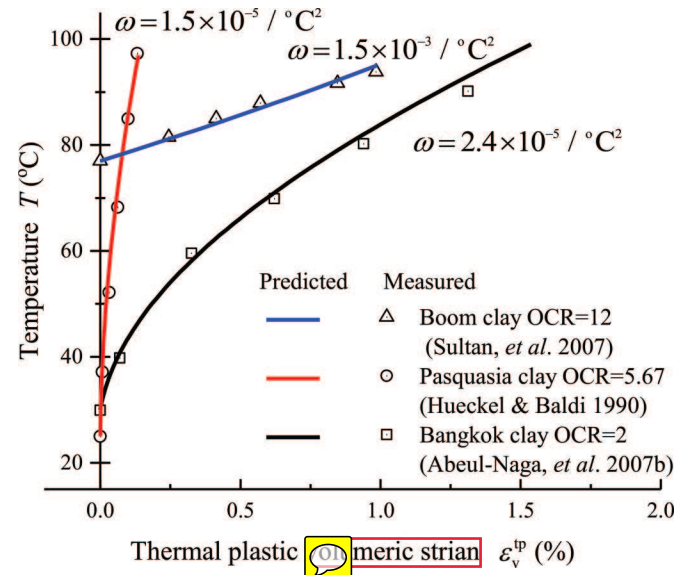
$$(16) \quad d\lambda_m = - \left(\frac{\partial f^{MY}}{\partial p} dp + \frac{\partial f^{MY}}{\partial q} dq + \frac{\partial f^{MY}}{\partial T} dT \right) / \left(\frac{\partial f^{MY}}{\partial p_{c(T_0)}} \frac{\partial p_{c(T_0)}}{\partial \varepsilon_v^{mp}} \frac{\partial g^{MY}}{\partial p} \right)$$

Upon heating, thermal plastic contraction occurs when the TY limit is reached. Experimental results (e.g., Abuel-Naga et al. (2007a), Baldi et al. (1991), Laloui and François (2009), Sultan et al. (2002)) indicated that the thermally induced plastic volumetric strain highly depends on the OCR value in addition to temperature changes (Cui et al. 2000; Graham et al. 2001; Hong et al. 2016; Yao and Zhou 2013). Furthermore, Demars and Charles (1982) and Sultan et al. (2002) reported that the thermal plastic volumetric strain (ε_v^{tp}) is independent of the magnitude of the effective confining stress applied. According to these findings, eq. 17 with only one additional material parameter is proposed and used to predict ε_v^{tp} .

$$(17) \quad d\varepsilon_v^{tp} = \omega(T - T_0) \left[\frac{p}{p_{c(T_0)}} \right]^2 dT$$

where ω is a soil parameter controlling the development of ε_v^{tp} and is assumed to be constant. Equation 17 is triggered only when the TY surface (eq. 12) is reached. In eq. 17 the hardening–

Fig. 7. Measured and predicted thermal plastic volumetric strains. [Colour online.]



softening of $p_{c(T_0)}$ is involved (e.g., eq. 18). Together with eq. 9, it can be seen that the thermally induced plastic volumetric strain defined here is a function of the temperature change and the current soil stress state (i.e., OCR), which is consistent with the abovementioned literature. Excellent agreement is shown in Fig. 7 between predicted and measured results of ε_v^{tp} for different soils at various stress conditions, which directly confirms the rationality of eq. 17.

Thermomechanical hardening laws and coupling mechanism

The preconsolidation pressure $p_{c(T_0)}$ appears in both the mechanical (i.e., eqs. 4 and 9) and the TY functions (i.e., eq. 12) as a hardening parameter. It is postulated that $p_{c(T_0)}$ depends on the total plastic volumetric strains (ε_v^p) as defined in eq. 18, and, thus, these two plastic mechanisms are coupled through ε_v^p . Mechanical and thermal plastic volumetric strains will move the MY and TY limits simultaneously.

$$(18) \quad dp_{c(T_0)} = p_{c0(T_0)} \frac{1 + e_0}{\lambda - \kappa} d\varepsilon_v^p$$

$$(19) \quad d\varepsilon_v^p = d\varepsilon_v^{tp} + d\varepsilon_v^{mp}$$

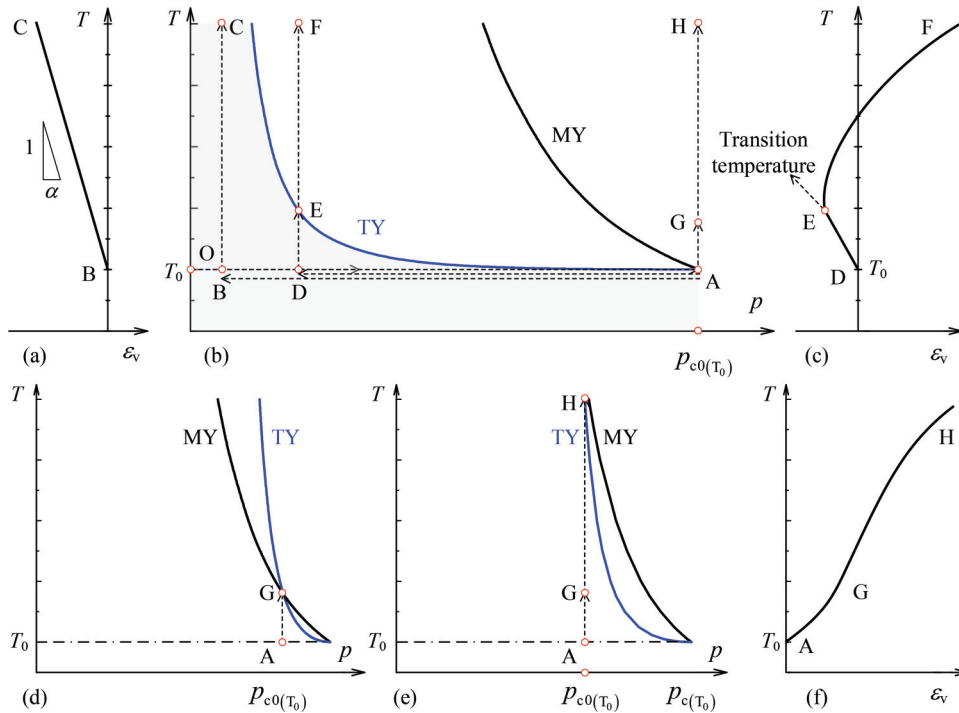
where $p_{c0(T_0)}$ is the initial preconsolidation pressure at the reference temperature T_0 .

The volumetric hardening (i.e., eq. 18) mainly affects the sizes or positions of the MY and TY curves. Meanwhile, their shapes may also vary with temperature due to thermal evolutions of the stress spacing ratio (see eq. 10) and the parameter β . While the TY mechanism is activated, a hardening phenomenon moves the TY surface upwards in the T - p plane as β reduces (see Fig. 5). The evolution of β can be determined from the consistency condition of TY function, as follows:

$$(20) \quad df^{TY} = \frac{\partial f^{TY}}{\partial p} dp + \frac{\partial f^{TY}}{\partial T} dT + \frac{\partial f^{TY}}{\partial \beta} d\beta + \frac{\partial f^{TY}}{\partial p_{c(T_0)}} dp_{c(T_0)} = 0$$

Mechanical plastic strains will develop when the MY mechanism is activated as defined in eqs. 13, and thermal plastic volumetric strains will be induced due to temperature changes as defined in eq. 17. In this model, the thermomechanical soil

Fig. 8. Explanation of model responses subjected to heating at three typical OCR values: (a) XXXX; (b) XXXX; (c) XXXX; (d) XXXX; (e) XXXX; (f) XXXX. [Colour online.]



response is loading path dependent. For example, although the TY curve will not be activated upon purely isothermal loading in the proposed model, thermal evolutions of the preconsolidation pressure and the spacing ratio possibly occurred during pre-thermal loadings. As a result, the isothermal strength of soil may either increase or decrease, depending on the stress and temperature history. For illustration, thermal evolutions of the MY and TY curves are discussed in the p - T plane along three typical drained thermal loading paths (e.g., from T_0 to T in Fig. 8) as follows:

Loading path: OABC

For heavily overconsolidated soils (e.g., point B), only recoverable thermal expansion occurs upon heating within the concerned temperature range (e.g., path $B \rightarrow C$). As the elastic thermal expansion coefficient α was assumed to be constant in eq. 7, the soil volume increases or decreases linearly during drained heating or cooling (e.g., Fig. 8a). As no plastic volumetric strain will be produced along this typical path, the preconsolidation pressure reduces at higher temperatures as defined by eq. 9.

Loading path: OADEF

At point D, the soil is intermediately overconsolidated. Upon heating from room temperature, thermal expansion dominates before reaching the TY limit (i.e., path $D \rightarrow E$ in Fig. 8b). Afterwards, thermal plastic deformation develops beyond the transition temperature (i.e., point E), and, therefore, $p_{c(T)}$ evolves. As thermal plastic deformation accumulates, a reduction of the soil volume will be caused (e.g., Fig. 8c). Overall, along with the path $D \rightarrow E \rightarrow F$, thermal expansion occurs first, followed by contractions. The transition temperature gets higher with greater OCR values as that has been widely observed in soil heating tests (Abuel-Naga et al. 2007b; Baldi et al. 1988; Cekerevac and Laloui 2004; Sultan et al. 2002).

Loading path: OAGH

At point A (normally consolidated state at room temperature), the proposed MY and TY coincides, and both of them are reached immediately. Upon heating from point A, $p_{c(T)}$ evolves as both plastic strain hardening and thermal softening occur, and, therefore, the locations of the MY and TY curves move as defined by eqs. 9 and 12, respectively. It is found that both the TY and MY limits will be reached along the heating path from A to G in the coupled hardening mechanism defined. Hence, both thermal and mechanical plastic strains develop, and the consistency conditions of eqs. 16 and 20 must be satisfied simultaneously. From G to H, the soil contraction is solely caused by thermal plastic deformation as only the TY mechanism is triggered. In other words, the soil always stays as normally consolidated under thermal loading in the temperature range between T_A and T_G (temperatures at points A and G, respectively), which is consistent with the test observation of Plum and Esrig (1969) in heating tests on Newfield clay from 24 to 50 °C; thermally induced overconsolidation effect is predicted with further temperature rise as the TY limit is always reached prior to the MY limit along G to H, which agrees well with experimental observations (Abuel-Naga et al. 2007a; Burghignoli et al. 1992; Sultan et al. 2002). As a result, an s-shape T - ϵ_v curve is predicted by the present model as illustrated in Fig. 8f. The range of path $A \rightarrow G$ might be soil specific (Sultan et al. 2002).

Determination of model parameters

There are a total number of 12 parameters required in the proposed model. The isothermal parameters (λ , κ , M , μ , $\Gamma_{(T)}$, n , and $r_{(T)}$) are similar to those of the mother model of CASM, the first five of which are common soil parameters of Cam-clay models. The determination procedure and typical values of the parameters were elaborated by Yu (1998). Under non-isothermal conditions, $r_{(T)}$ and $\Gamma_{(T)}$ were assumed to be temperature dependent, which can be calculated by eqs. 10 and 21, respectively.

AQ16

AQ6

F8

$$(21) \quad \Gamma_{(T)} = \Gamma_{(T_0)} - (\lambda - \kappa)(\theta - \zeta) \ln(T/T_0)$$

New soil parameters that are introduced to account for the temperature effects include α , θ , ζ , β_0 , and ω . The role of each of them and practical methods for determining them are briefly discussed as follows.

1. The elastic thermal expansion coefficient α can be calibrated from the cooling stage of a drained heating-cooling test or a drained heating test on a heavily overconsolidated soil in the T - ε_v plot. α is mainly determined by the thermal expansion coefficient of the solid constituent (Khalili et al. 2010) and can be considered as constant in the order of $10^{-5} \text{ }^\circ\text{C}^{-1}$ for most practical purposes.
2. As defined in eq. 9, θ controls the temperature dependency of the preconsolidation pressure at a constant plastic strain, which is generally of positive value. It can be obtained by performing two or more isotropic compression tests at different constant temperatures.
3. β_0 determines the initial shape or position of the TY curve in the p - T plot (e.g., Fig. 5). The transition temperature at a given OCR can be determined by plotting isotropic drained heating test results in the ε_v - T plot (e.g., Fig. 8c). With measured values of the transition temperature at different OCRs (at least two), β_0 can be fitted using eq. 11.
4. The spacing ratio typically lies in the range of 1.5~3.0 for clays (Yu 1998), which can be determined by locating the NCL and the CSL at a given temperature. The thermal evolution of $r_{(T)}$ is controlled by the parameter ζ as defined in eq. 10. With measured values of $r_{(T)}$ at different temperatures (at least two), ζ can be obtained by the method of fitting in the $r_{(T)}$ - T plot (e.g., Fig. 3). Alternatively, as the spacing ratio defines the shape of the MY surface, the relationship between $r_{(T)}$ and T can also be estimated by fitting the yield loci obtained at different temperatures.
5. In eq. 17, ω controls the development of thermal plastic strain. It can be calibrated from thermal isotropic drained heating tests (e.g., Fig. 7).

In the preceding procedure, both one-dimensional (1D) compression and three dimensional (3D) triaxial tests at a range of temperatures are involved to determine the soil parameters. Alternatively, the whole set of parameters can be efficiently identified with a limited number of 3D conventional soil tests (e.g., triaxial tests at different temperatures) using an appropriate optimization method (Jin et al. 2017; Mattsson et al. 1999; Yin et al. 2017). In general, the optimization procedure consists of two core parts: (i) the definition of an error function measuring the difference between model responses and experimental results and (ii) the selection of an optimization strategy to enable the search for the minimum of this error function (Yin et al. 2018).

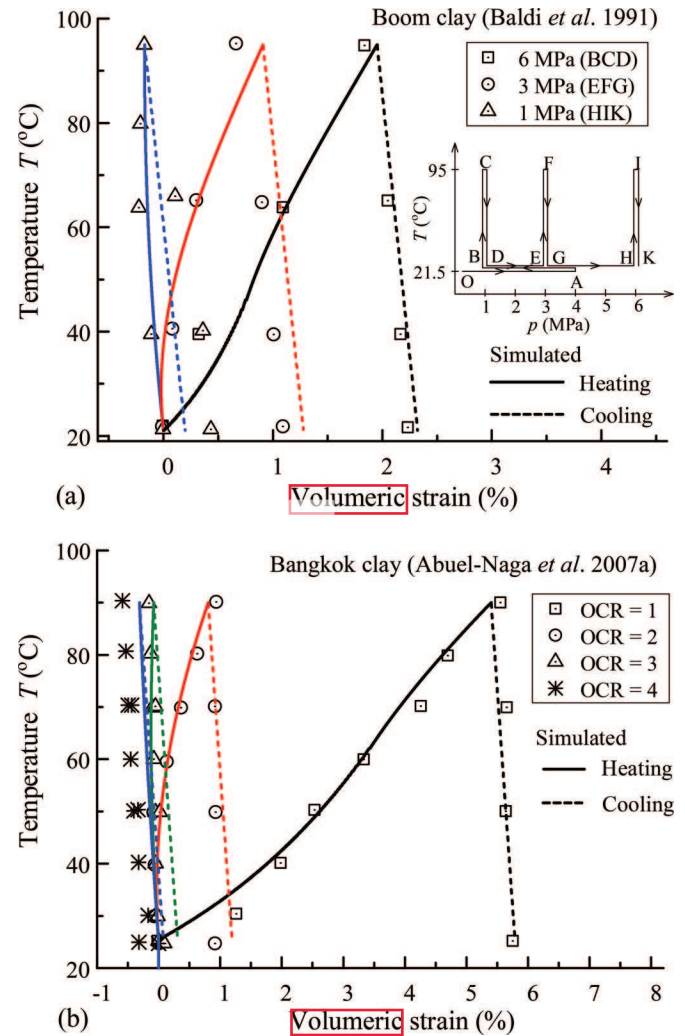
Evaluation of proposed model

To test the reliability of the proposed model, predictions of various short-term thermomechanical behaviours of soils are compared with experimental data published in the literature. Note that the simulations of these soil element tests were performed at the element level, namely the distributions of strains and temperature were regarded as uniform throughout the soil element. Model parameters for each soil were calibrated following the preceding procedure based on test data, and they are summarized in Table 1.

Temperature effect on drained volumetric behaviour

Thermally induced volume changes of natural Boom clay and reconstituted Bangkok clay subjected to heating-cooling cycles at different OCRs were simulated, and they are compared with

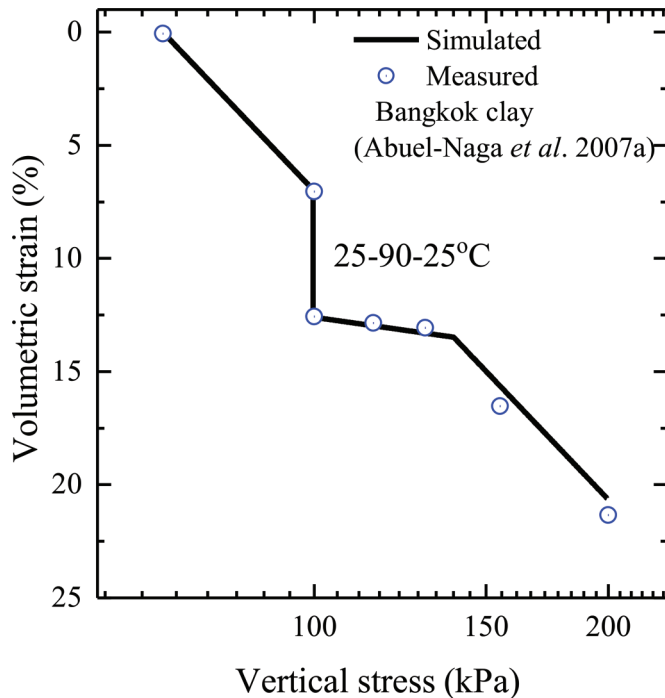
Fig. 9. Measured and simulated thermal volumetric deformation under heating-cooling cycle at different OCRs: (a) natural Boom clay ($e_0 = 0.59$); (b) Bangkok clay ($e_0 = 1.4$). [Colour online.]



experimental results of Baldi et al. (1991) and Abuel-Naga et al. (2007a) in Fig. 9. In the tests of Baldi et al. (1991), the Boom clay was saturated under a constant $p = 2$ MPa first, then isotropically loaded up to 4 MPa, and unloaded to 1 MPa prior to heating. After, three heating-cooling cycles of 21.5–95–21.5 °C were applied under $p = 1, 3, 6$ MPa (OCR = 4, 1.33, 1, respectively) with a continuous test procedure as depicted in Fig. 9a. The adopted tests of Abuel-Naga et al. (2007a) (Fig. 9b) were performed in a similar manner. The soil samples were consolidated under a vertical stress of 200 kPa and unloaded to be different stress levels (giving OCR = 1, 2, 4, and 8), followed by an incremental heating-cooling cycle of 22–90–22 °C.

Taking the tests of Baldi et al. (1991) as an example, the thermal related parameters α , β_0 , and ω were calibrated based on the data during the heating stage at $p = 1$ MPa; $\theta = 0.24$ was determined as the preconsolidation pressures were 6 and 4.2 MPa at 21.5 and 95 °C, respectively; other parameters were measured by Baldi et al. (1991) as summarized in Table 1. Note that two methods were used to calculate the drained thermal volumetric strain in the test. The results that subtracted the thermal expansion of both the pore water and the solid phase from the measured volume of water expelled from the soil sample were used in Fig. 9a because they are believed more accurate as discussed by Hong

Fig. 10. Measured and simulated consolidation curves under combined thermomechanical oedometric path. [Colour online.]



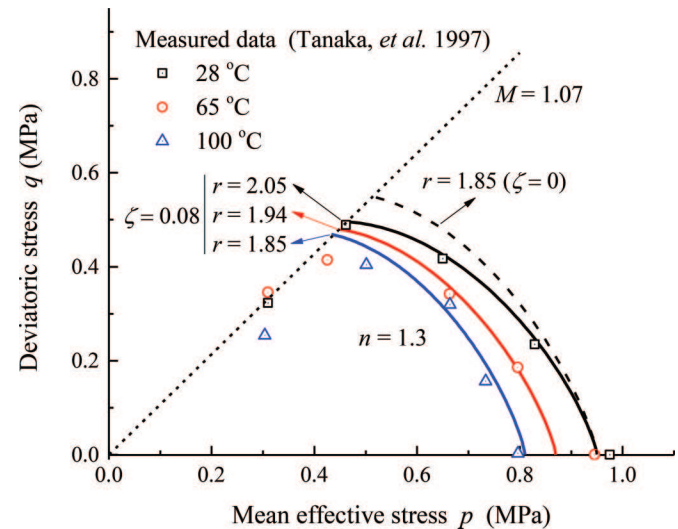
et al. (2013). Overall, great effects of stress history on the thermal volumetric strain under drained heating-cooling cycles are shown in Fig. 9, and the predicted and measured results were in good agreement at different OCRs. This demonstrates the model's capacity in capturing these effects, and the mechanisms were elaborated in Fig. 8.

F10 Figure 10 shows a comparison between simulated and measured results of Bangkok clay on a combined thermomechanical path. The test consists in oedometric loading of the normally consolidated Bangkok clay until an effective vertical stress of 100 kPa, followed by a heating-cooling cycle of 22–90–22 °C and finishing at vertical loading up to 200 kPa. (Abuel-Naga et al. 2007a). An apparent overconsolidation state after one heating-cooling cycle was caused, which is in line with other observations in the literature (e.g., Burghignoli et al. (1992), Sultan et al. (2002)). Using the soil parameters in Table 1, this thermally induced overconsolidation behaviour is also well predicted by the proposed model (Fig. 10).

Undrained triaxial compression tests at different temperatures

Tanaka (1995) reported several undrained triaxial compression tests on reconstituted illite clay at different temperatures. In the tests, three normally consolidated specimens were prepared by increasing the effective consolidation pressure to 1.5 MPa at $T_0 = 28$ °C; two overconsolidated specimens were produced by applying an effective consolidation pressure up to 1 MPa followed by isotropic unloading to 0.5 MPa, giving OCR = 2. After initial consolidations, the specimens were heated to desired temperatures under drained conditions. Finally, undrained triaxial shear tests were performed with the normally consolidated specimens at three constant temperatures (i.e., 28, 65, and 100 °C) and with the overconsolidated specimens at two constant temperatures (i.e., 28 and 65 °C). The calibrated model parameters are listed in Table 1. It should be noted that the stress-state coefficient n and the spacing ratio were obtained by fitting the measured yield limits on the

Fig. 11. Measured and predicted yield loci for illite clay. [Colour online.]



“wet” side as shown in Fig. 11; $\omega = 0.6 \times 10^{-6} \text{ } ^\circ\text{C}^2$ was fitted with the **AQ7** experimental results on the normally consolidated sample at $T = 65$ °C; typical values of α and β_0 were assumed as related data of thermal isotropic tests were not available in the reference.

Numerical simulations were performed following the same loading paths as those were applied in the tests. Good agreement between the measured and predicted stress-strain curves is shown in Fig. 12. The results show that the normally consolidated illite clay has greater undrained shear strength and generated lower pore-water pressures at higher temperatures, and the difference becomes smaller for samples of OCR = 2. The predicted yield loci in Fig. 11 indicate that the peak shear strength at high OCR may turn to decrease with increasing temperature, and this has also been observed in similar tests on different soils (De Bruyn and Thimus 1996; Hueckel and Borsetto 1990). The predicted and measured stress paths of the normally consolidated soil samples at different temperatures are compared in Fig. 13. Apparent thermal overconsolidation behaviour at elevated temperatures are shown due to the thermal evolution of the MY surface as explained in Fig. 8 (e.g., path OAGH). As the soil response is assumed as purely elastic within the SBS (i.e., elastic wall) in the present model, which is described by using a simple hypoelastic model (i.e., eqs. 7 and 8), the predicted transition from elastic to elastoplastic states is unnecessarily abrupt. This issue can be readily tackled by introducing the bounding surface scheme (Dafalias 1986; Laloui and François 2009; Zhou and Ng 2015) or empirical relationships accounting for soil stiffness degradation (Hardin and Black 1968; Vardanega and Bolton 2013). Meanwhile, this will also give a more accurate prediction of the stress path for the test at 100 °C. To minimize the number of model parameters, they were not included in this basic model.

It is shown in Fig. 12 that, for normally consolidated specimens at elevated temperatures, the peak deviatoric stresses are slightly underestimated, and excess pore-water pressures (Δu) are therefore overpredicted. In the framework of critical state soil mechanics, no further volumetric plastic strains will be generated at the critical state. Hence, constant critical-state values of q and Δu were predicted by soil models with the volumetric hardening mechanism only, which agree well with the test results at room temperature (e.g., $T = 2.8$ °C in Fig. 13). However, as shown in Fig. 13, hardening continued at the critical state for the specimens at elevated temperatures, and the hardening effect was more significant

Fig. 12. Measured and simulated stress–strain curves for undrained triaxial tests on soft illite clay at different temperatures (measured data from Tanaka 1995). [Colour online.]

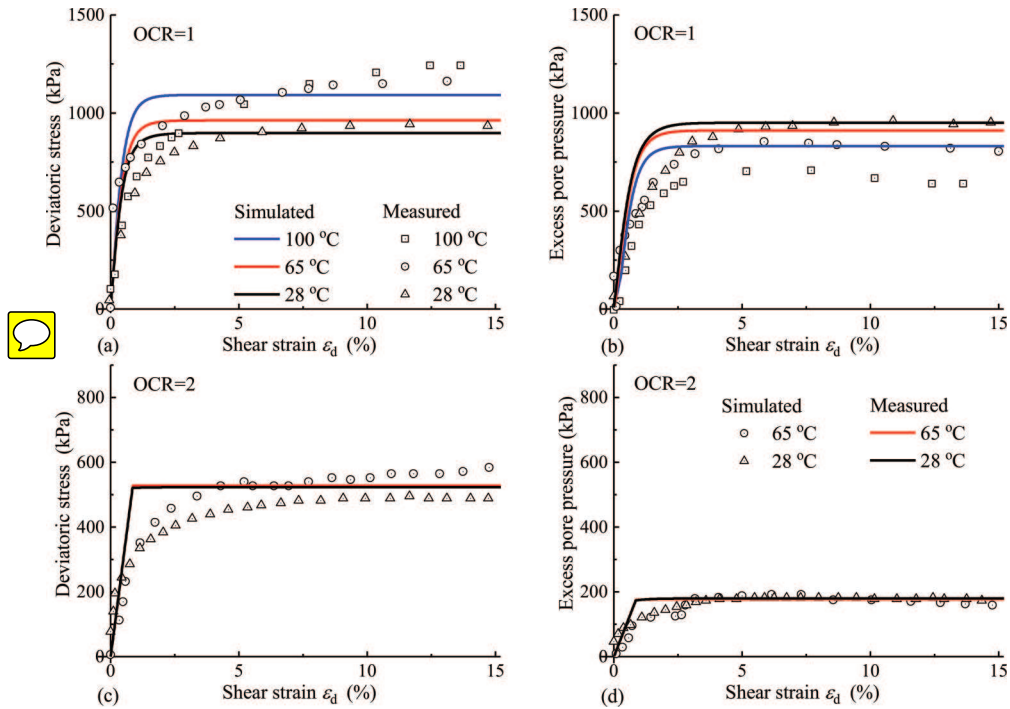
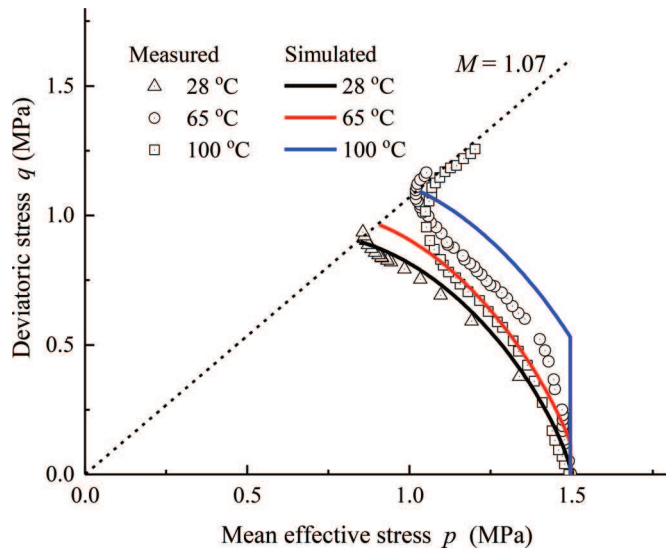
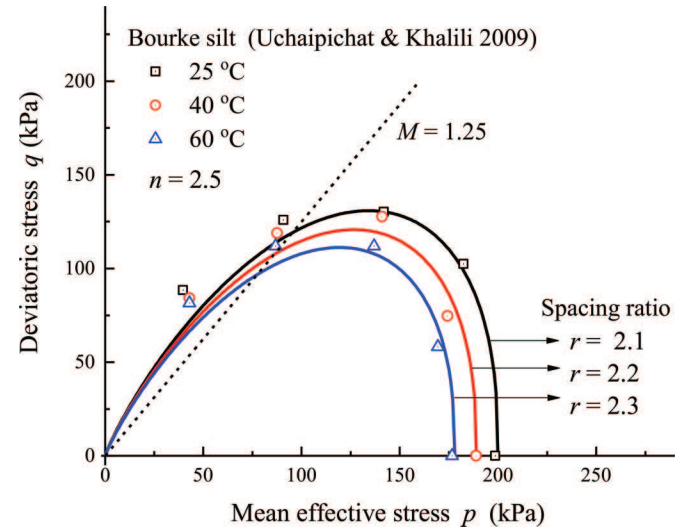


Fig. 13. Measured and predicted stress paths for normally consolidated illite clay in undrained triaxial compression tests (measured data from Tanaka 1995). [Colour online.]



at $T = 100 \text{ }^\circ\text{C}$. This phenomenon may be related to thermally induced anisotropy due to the heterogeneity of clay. However, it is important to note that the finding on this temperature-related hardening phenomenon at the critical state is not conclusive in the literature, e. g., an opposite trend was reported by Abuel-Naga et al. (2007b) in undrained triaxial tests on soft Bangkok clay. In theory, it is anticipated that this behaviour can be modelled by adopting more complex hardening laws with inclusion of additional contributions from plastic shear strains (e.g., combined deviatoric and volumetric hardening laws) (Collins and Kelly 2002; Dafalias and Taiebat 2013; Wheeler et al. 2003; Yu et al. 2005).

Fig. 14. Measured and predicted yield loci for Bourke silt. [Colour online.]

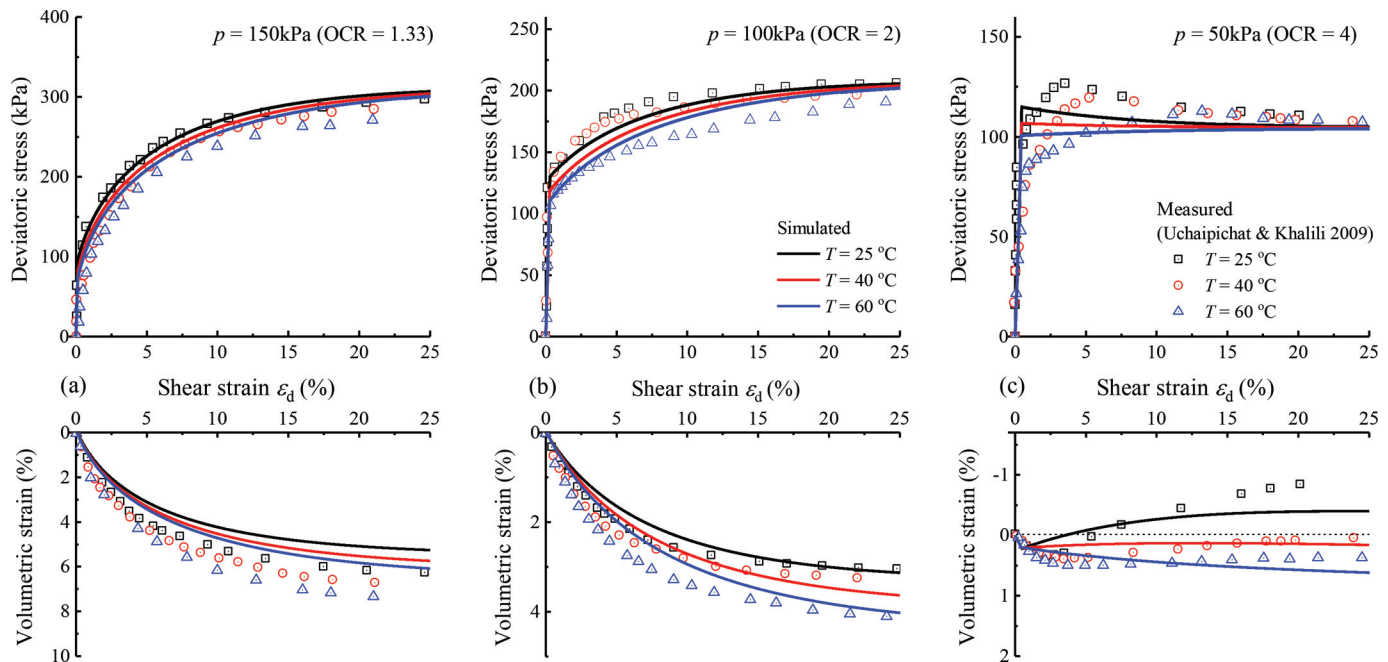


Drained triaxial compression tests at different temperatures

Drained triaxial compression tests on saturated Bourke silt at different temperatures reported by Uchaipichat and Khalili (2009) were simulated and compared in Figs. 14 and 15. Nine soil specimens were initially consolidated under an isotropic loading of 200 kPa at 25 °C, followed by unloading to 150, 100, or 50 kPa (i.e., OCR = 1.33, 2, 4). Then some of them were heated to 40 or 60 °C under drained condition prior to performing isothermal drained triaxial compression tests. Note that the model parameters α , β_0 , and ω were determined by fitting the results of OCR = 2 at $T = 40 \text{ }^\circ\text{C}$; n , $r_{(T)}$, and ζ were calibrated by fitting the measured yield loci as shown in Fig. 14. Note that the yielding points at high

F14-F15

Fig. 15. Measured and predicted stress behaviour of Bourke silt in drained triaxial compression tests ($e_0 = 0.56$). (a) XXXX; (b) XXXX; (c) XXXX. [Colour online.]



OCR values are underestimated, and this leads to underestimations of the peak strength for tests at OCR = 4 (Fig. 15c).

For the Bourke silt, it was measured that the spacing ratio increases with an increase in temperature (e.g., Fig. 14). This behaviour is also reflected in the plot of volumetric strain versus shear strain (e.g., Fig. 15c). It is shown that the amount of shear dilation of soil at OCR = 4 (strain softening) is smaller at higher temperatures, and this can be well captured by the proposed flow rule (eq. 14) with a negative value of ζ . In the drained triaxial shear tests of the Bourke silt (Fig. 14), the shear stress reduces with the increase of the temperature before reaching the critical state, where the temperature effects on the stress path almost vanish. On the contrary, the temperature effects on the volumetric strain accumulate with shear strain, and the soil deformation becomes more contractive at a higher temperature. Although the volumetric strains at OCR = 1.33 and the peak strength at OCR = 4 was slightly underestimated, overall soil behaviours are well reproduced by the model simulations, which confirms the validity of the proposed model for drained triaxial shear tests at different temperatures.

Conclusions

In this paper, a two-surface (TY coupled with MY) based elastoplastic constitutive model is developed in the critical state framework for describing the thermomechanical behaviour of saturated fine-grained soils. The TY and MY mechanisms are coupled through the volumetric plastic strain which is expressed in terms of both stress and temperature. To better characterize the isotropic thermal deformation of soil, a TY surface is introduced and a new expression for the thermoplastic strains is proposed and validated. Both the size and the shape of the MY surface are allowed to vary with temperature, which are dependent on the combined hardening mechanism of the preconsolidation pressure and the thermal dependent spacing ratio, respectively. A nonlinear relationship between the spacing ratio and temperature changes is defined based on available experimental observations. The soil stress dilatancy is related to the spacing ratio as well, thus a non-associated thermal dependent plastic potential is obtained, by

which some observed temperature effects on the flow rule are well captured. The number of model parameters is kept to a minimum. All the parameters have a clear physical interpretation, and a detailed procedure for determining each of them is presented.

The model is evaluated by comparing it with selected experimental results of several typical stress and temperature-controlled tests. It is demonstrated that many important thermomechanical features of saturated soils at non-isothermal conditions can be well described by the model, e.g., thermal deformation of soil at different OCRs in one heating-cooling cycle, thermally induced overconsolidation effect observed in normally consolidated soils, and thermally induced soil strength changes (either increase or decrease) in both undrained and drained triaxial shear tests. It also reveals that further experimental and constitutive investigations, particularly, into the microscopic behaviour and mechanisms, are necessarily needed for better explaining and modelling some contrasting phenomena related to coupled thermal and mechanical effects.

Acknowledgement

The authors would like to acknowledge the National Natural Science Foundation of China (41502271), the State Key Laboratory for GeoMechanics and Deep Underground Engineering China University of Mining and Technology (SKLGDUEK1802), and the International Mobility Fund from the University of Leeds, which collectively supported this project. The second author also acknowledges the support of the "Taishan" Scholar Program of Shandong Province, China (No. tsqn201909016) and the "Qilu" Scholar Program of Shandong University.

References

- Abuel-Naga, H., Bergado, D., Bouazza, A., and Ramana, G. 2007a. Volume change behaviour of saturated clays under drained heating conditions: experimental results and constitutive modeling. *Canadian Geotechnical Journal*, 44(8): 942–956. doi:10.1139/t07-031.
- Abuel-Naga, H.M., Bergado, D.T., and Lim, B.F. 2007b. Effect of temperature on shear strength and yielding behavior of soft Bangkok clay. *Soils and Foundations*, 47(3): 423–436. doi:10.3208/sandf.47.423.

- Abuel-Naga, H., Bergado, D., Bouazza, A., and Pender, M. 2009. Thermomechanical model for saturated clays. *Géotechnique*, **59**(3): 273–278. doi:10.1680/geot.2009.59.3.273.
- Bai, B., Yang, G., Li, T., and Yang, G. 2019. A thermodynamic constitutive model with temperature effect based on particle rearrangement for geomaterials. *Mechanics of Materials*, **139**: 103180. doi:10.1016/j.mechmat.2019.103180.
- Baldi, G., Hueckel, T., and Pellegrini, R. 1988. Thermal volume changes of the mineral-water system in low-porosity clay soils. *Canadian Geotechnical Journal*, **25**(4): 807–825. doi:10.1139/t88-089.
- Baldi, G., Hueckel, T., Peano, A., and Pellegrini, R. 1991. Developments in modelling of thermohydro-geomechanical behaviour of Boom clay and clay-based buffer materials (Volume 1). EUR 13365/1. Commission of the European Communities, Luxembourg.
- Barla, M., Di Donna, A., and Perino, A. 2016. Application of energy tunnels to an urban environment. *Geothermics*, **61**: 104–113. doi:10.1016/j.geothermics.2016.01.014.
- Been, K., and Jefferies, M.G. 1985. A state parameter for sands. *Géotechnique*, **35**(2): 99–112. doi:10.1680/geot.1985.35.2.99.
- AQ12** Bourne-Webb, P., Amatya, B., Soga, K., Amis, T., Davidson, C., and Payne, P. 2009. Energy pile test at Lambeth College, London: geotechnical and thermodynamic aspects of pile response to heat cycles. *Géotechnique*, **59**(3): 237–248. doi:10.1680/geot.2009.59.3.237.
- Bourne-Webb, P., Burlon, S., Javed, S., Kürten, S., and Loveridge, F. 2016. Analysis and design methods for energy geostructures. *Renewable and Sustainable Energy Reviews*, **65**: 402–419. doi:10.1016/j.rser.2016.06.046.
- Bourne-Webb, P., Freitas, T.B., and Assunção, R.F. 2019. A review of pile-soil interactions in isolated, thermally-activated piles. *Computers and Geotechnics*, **108**: 61–74. doi:10.1016/j.compgeo.2018.12.008.
- Burghignoli, A., Desideri, A., and Miliziano, S. 1992. Deformability of clays under non isothermal conditions. *Rivista Italiana di Geotecnica*, **92**(4): 227–236.
- Campanella, R.G., and Mitchell, J.K. 1968. Influence of temperature variations on soil behavior. *Journal of Soil Mechanics and Foundations Division*, **94**: 709–734.
- Cekerevac, C., and Laloui, L. 2004. Experimental study of thermal effects on the mechanical behaviour of a clay. *International Journal for Numerical and Analytical Methods in Geomechanics*, **28**(3): 209–228. doi:10.1002/nag.332.
- Chen, G., Chenevert, M.E., Sharma, M.M., and Yu, M. 2003. A study of wellbore stability in shales including poroelastic, chemical, and thermal effects. *Journal of Petroleum Science and Engineering*, **38**(3–4): 167–176. doi:10.1016/S0920-4105(03)00030-5.
- Coccia, C.J.R., and McCartney, J.S. 2016. Thermal volume change of poorly draining soils II: model development and experimental validation. *Computers and Geotechnics*, **80**: 16–25. doi:10.1016/j.compgeo.2016.06.010.
- Collins, I.F., and Kelly, P.A. 2002. A thermomechanical analysis of a family of soil models. *Géotechnique*, **52**(7): 507–518. doi:10.1680/geot.2002.52.7.507.
- Cui, Y.J., Sultan, N., and Delage, P. 2000. A thermomechanical model for saturated clays. *Canadian Geotechnical Journal*, **37**(3): 607–620. doi:10.1139/t99-111.
- Dafalias, Y.F. 1986. Bounding surface plasticity. I: Mathematical foundation and hypoplasticity. *Journal of Engineering Mechanics*, **112**(9): 966–987. doi:10.1061/(ASCE)0733-9399(1986)112:9(966).
- Dafalias, Y.F., and Taiebat, M. 2013. Anatomy of rotational hardening in clay plasticity. *Géotechnique*, **63**(16): 1406–1418. doi:10.1680/geot.12.P.197.
- Demars, K., and Charles, R. 1982. Soil volume changes induced by temperature cycling. *Canadian Geotechnical Journal*, **19**(2): 188–194. doi:10.1139/t82-021.
- Di Donna, A., Cecinato, F., Loveridge, F., and Barla, M. 2017. Energy performance of diaphragm walls used as heat exchangers. *Proceedings of the Institution of Civil Engineers - Geotechnical Engineering*, **170**(3): 232–245. doi:10.1680/jgeen.16.00092.
- di Schio, E.R., Lazzari, S., and Abbati, A. 2016. Natural convection effects in the heat transfer from a buried pipeline. *Applied Thermal Engineering*, **102**: 227–233.
- Eriksson, L. 1989. Temperature effects on consolidation properties of sulphide clays. In *Proceedings of the 12th International Conference on Soil Mechanics and Foundation Engineering*, Rio de Janeiro. pp. 2087–2090.
- Gahremannejad, B. 2003. Thermo-mechanical behaviour of two reconstituted clays. University of Sydney, Sydney, Australia.
- Graham, J., Chandler, N.A., Dixon, D.A., Roach, P.J., To, T., and Wan, A.W.L. 1997. The buffer/container experiment: results, synthesis, issues. Whiteshell Laboratories Atomic Energy of Canada Limited Report AECL 11746 and CANDU Owners Group Report COG-97-46-1, Pinawa, Manitoba.
- Graham, J., Tanaka, N., Crilly, T., and Alfaro, M. 2001. Modified Cam-Clay modelling of temperature effects in clays. *Canadian Geotechnical Journal*, **38**(3): 608–621. doi:10.1139/t00-125.
- Hamidi, A., and Khazaei, C. 2010. A thermo-mechanical constitutive model for saturated clays. *International Journal of Geotechnical Engineering*, **4**(4): 445–459. doi:10.3328/IJGE.2010.04.04.445-459.
- Hamidi, A., Tourchi, S., and Khazaei, C. 2015. Thermomechanical constitutive model for saturated clays based on critical state theory. *International Journal of Geomechanics*, **15**(1): 04014038. doi:10.1061/(ASCE)GM.1943-5622.0000402.
- Hardin, B.O., and Black, W.L. 1968. Vibration modulus of normally consolidated clay. *Journal of the Soil Mechanics and Foundations Division*, **94**(2): 353–370.
- Hong, P., Pereira, J., Tang, A., and Cui, Y.-J. 2013. On some advanced thermomechanical models for saturated clays. *International Journal for Numerical and Analytical Methods in Geomechanics*, **37**(17): 2952–2971. doi:10.1002/nag.2170.
- Hong, P.Y., Pereira, J.-M., Cui, Y.J., and Tang, A.M. 2016. A two-surface thermomechanical model for saturated clays. *International Journal for Numerical and Analytical Methods in Geomechanics*, **40**(7): 1059–1080. doi:10.1002/nag.2474.
- Hong, Y., Wang, L., Zhang, J., and Gao, Z. 2020. 3D elastoplastic model for fine-grained gassy soil considering the gas-dependent yield surface shape and stress-dilatancy. *Journal of Engineering Mechanics*, **146**(5): 04020037. doi:10.1061/(ASCE)EM.1943-7889.0001760.
- Hueckel, T., and Baldi, G. 1990. Thermoplasticity of saturated clays: experimental constitutive study. *Journal of Geotechnical Engineering*, **116**(12): 1778–1796. doi:10.1061/(ASCE)0733-9410(1990)116:12(1778).
- Hueckel, T., and Borsetto, M. 1990. Thermoplasticity of saturated soils and shales: constitutive equations. *Journal of Geotechnical Engineering*, **116**(12): 1765–1777. doi:10.1061/(ASCE)0733-9410(1990)116:12(1765).
- Hueckel, T., and Pellegrini, R. 1991. Thermoplastic modeling of undrained failure of saturated clay due to heating. *Soils and Foundations*, **31**(3): 1–16. doi:10.3208/sandf1972.31.3.1.
- Hueckel, T., François, B., and Laloui, L. 2009. Explaining thermal failure in saturated clays. *Géotechnique*, **59**(3): 197–212. doi:10.1680/geot.2009.59.3.197.
- Jin, Y.-F., Wu, Z.-X., Yin, Z.-Y., and Shen, J.S. 2017. Estimation of critical state-related formula in advanced constitutive modeling of granular material. *Acta Geotechnica*, **12**(6): 1329–1351. doi:10.1007/s11440-017-0586-5.
- Khalili, N., Uchaipichat, A., and Javadi, A. 2010. Skeletal thermal expansion coefficient and thermo-hydro-mechanical constitutive relations for saturated homogeneous porous media. *Mechanics of Materials*, **42**(6): 593–598. doi:10.1016/j.mechmat.2010.04.001.
- Kuntiwattanukul, P., Towhata, I., Ohishi, K., and Seko, I. 1995. Temperature effects on undrained shear characteristics of clay. *Soils and Foundations*, **35**(1): 147–162. doi:10.3208/sandf1972.35.1.147.
- Laloui, L., and Cekerevac, C. 2003. Thermo-plasticity of clays: an isotropic yield mechanism. *Computers and Geotechnics*, **30**(8): 649–660. doi:10.1016/j.compgeo.2003.09.001.
- Laloui, L., and Di Donna, A. 2013. Energy geostructures: innovation in underground engineering. John Wiley & Sons.
- Laloui, L., and François, B. 2009. ACMEG-T: soil thermoplasticity model. *Journal of Engineering Mechanics*, **135**(9): 932–944. doi:10.1061/(ASCE)EM.1943-7889.00000011.
- Laloui, L., Nuth, M., and Vulliet, L. 2006. Experimental and numerical investigations of the behaviour of a heat exchanger pile. *International Journal for Numerical and Analytical Methods in Geomechanics*, **30**(8): 763–781. doi:10.1002/nag.499.
- Li, X., Feng, Y., El Mohtar, C.S., and Gray, K. 2019. Transient modeling of borehole breakouts: A coupled thermo-hydro-mechanical approach. *Journal of Petroleum Science and Engineering*, **172**: 1014–1024. doi:10.1016/j.petrol.2018.09.008.
- Lingnau, B., Graham, J., and Tanaka, N. 1995. Isothermal modeling of sand-bentonite mixtures at elevated temperatures. *Canadian Geotechnical Journal*, **32**(1): 78–88. doi:10.1139/t95-006.
- Liu, E.L., and Xing, H.L. 2009. A double hardening thermo-mechanical constitutive model for overconsolidated clays. *Acta Geotechnica*, **4**(1): 1–6. doi:10.1007/s11440-008-0053-4.
- Mašin, D., and Khalili, N. 2012. A thermo-mechanical model for variably saturated soils based on hypoplasticity. *International Journal for Numerical and Analytical Methods in Geomechanics*, **36**(12): 1461–1485. doi:10.1002/nag.1058.
- Mattsson, H., Axelsson, K., and Klisinski, M. 1999. On a constitutive driver as a useful tool in soil plasticity. *Advances in Engineering Software*, **30**(8): 511–528. doi:10.1016/S0965-9978(99)00007-1.
- McDowell, G.R., and Hau, K.W. 2003. A simple non-associated three surface kinematic hardening model. *Géotechnique*, **53**(4): 433–437. doi:10.1680/geot.2003.53.4.433.
- Mitchell, J.K., and Abdel-Hadi, O. N. 1979. Temperature distributions around buried cables. *IEEE Transactions on Power Apparatus and Systems*, **PAS-98**(4): 1158–1166. doi:10.1109/TPAS.1979.319306.
- Moritz, L. 1995. Geotechnical properties of clay at elevated temperatures. Swedish Geotechnical Institute, Linköping, Sweden.
- Ng, C.W.W., Mu, Q., and Zhou, C. 2019. Effects of specimen preparation method on the volume change of clay under cyclic thermal loads. *Géotechnique*, **69**(2): 146–150. doi:10.1680/jgeot.16.P.293.
- Pinyol, N., Alvarado, M., Alonso, E., and Zabala, F. 2018. Thermal effects in landslide mobility. *Géotechnique*, **68**(6): 528–545. doi:10.1680/jgeot.17.P.054.
- Plum, R.L., and Esrig, M.I. 1969. Some temperature effects on soil compressibility and pore water pressure. Highway Research Board Special Report 103. Highway Research Board, Washington, D.C.
- Robinet, J.-C., Rahbaoui, A., Plas, F., and Lebon, P. 1996. A constitutive thermo-mechanical model for saturated clays. *Engineering Geology*, **41**(1–4): 145–169. doi:10.1016/0013-7952(95)00049-6.

- Roscoe, K.H., and Burland, J.B. 1968. On the generalized stress-strain behaviour of wet clay. In *Engineering plasticity*. Edited by G. Heymann and F.A. Leckie. Cambridge University Press, London, UK. pp. 535–609.
- Roscoe, K.H., Schofield, A.N., and Wroth, C.P. 1958. On the yielding of soils. *Géotechnique*, **8**(1): 22–53. doi:10.1680/geot.1958.8.1.22.
- Schofield, A.N., and Wroth, C.P. 1968. *Critical state soil mechanics*. McGraw-Hill, London.
- Seneviratne, H., Carter, J., Airey, D., and Booker, J. 1993. A review of models for predicting the thermomechanical behaviour of soft clays. *International Journal for Numerical and Analytical Methods in Geomechanics*, **17**(10): 715–733. doi:10.1002/nag.1610171004.
- Shetty, R., Singh, D., and Ferrari, A. 2019. Volume change characteristics of fine-grained soils due to sequential thermo-mechanical stresses. *Engineering Geology*, **253**: 47–54. doi:10.1016/j.enggeo.2019.03.008.
- Sultan, N., Delage, P., and Cui, Y. 2002. Temperature effects on the volume change behaviour of Boom clay. *Engineering Geology*, **64**(2): 135–145. doi:10.1016/S0013-7952(01)00143-0.
- Tanaka, N. 1995. *Thermal elastic plastic behaviour and modelling of saturated clays*. University of Manitoba, Winnipeg, Manitoba, Canada.
- Tanaka, N., Graham, J., and Crilly, T. 1997. Stress-strain behaviour of reconstituted illitic clay at different temperatures. *Engineering Geology*, **47**(4): 339–350. doi:10.1016/S0013-7952(96)00113-5.
- Teltayev, B., and Suppes, E. 2019. Temperature in pavement and subgrade and its effect on moisture. *Case Studies in Thermal Engineering*, **13**: 100363. doi:10.1016/j.csite.2018.11.014.
- Towhata, I., Kuntiwattanaku, P., Seko, I., and Ohishi, K. 1993. Volume change of clays induced by heating as observed in consolidation tests. *Soils and Foundations*, **33**(4): 170–183. doi:10.3208/sandf1972.33.4_170.
- Uchaipichat, A., and Khalili, N. 2009. Experimental investigation of thermo-hydro-mechanical behaviour of an unsaturated silt. *Géotechnique*, **59**(4): 339–353. doi:10.1680/geot.2009.59.4.339.
- Vardanega, P., and Bolton, M. 2013. Stiffness of clays and silts: Normalizing shear modulus and shear strain. *Journal of Geotechnical and Geoenvironmental Engineering*, ASCE, **139**(9): 1575–1589. doi:10.1061/(ASCE)GT.1943-5606.0000887.
- Wang, L., Wang, K., and Hong, Y. 2016. Modeling temperature-dependent behavior of soft clay. *Journal of Engineering Mechanics*, ASCE, **142**(8): 04016054. doi:10.1061/(ASCE)EM.1943-7889.0001108.
- Wheeler, S.J., Näätänen, A., Karstunen, M., and Lojander, M. 2003. An anisotropic elastoplastic model for soft clays. *Canadian Geotechnical Journal*, **40**(2): 403–418. doi:10.1139/t02-119.
- Wood, D.M. 1990. *Soil behaviour and critical state soil mechanics*. Cambridge University Press, Cambridge, UK.
- Wroth, C.P. 1984. The interpretation of in situ soil tests. *Géotechnique*, **34**(4): 449–489. doi:10.1680/geot.1984.34.4.449.
- Xiao, H. 2014. Thermo-coupled elastoplasticity models with asymptotic loss of the material strength. *International Journal of Plasticity*, **63**: 211–228. doi:10.1016/j.ijplas.2014.01.013.
- Yao, Y.P., and Zhou, A.N. 2013. Non-isothermal unified hardening model: a thermo-elasto-plastic model for clays. *Géotechnique*, **63**(15): 1328–1345. doi:10.1680/geot.13.P.035.
- Yao, Y.P., Hou, W., and Zhou, A.N. 2009. ~~UH model: three dimensional unified hardening model for overconsolidated clays. Géotechnique, 59(5): 451–469. doi:10.1680/geot.2007.00029.~~
- Yin, Z.Y., Jin, Y.F., Shen, S.-L., and Huang, H.W. 2017. An efficient optimization method for identifying parameters of soft structured clay by an enhanced genetic algorithm and elastic-viscoplastic model. *Acta Geotechnica*, **12**(4): 849–867. doi:10.1007/s11440-016-0486-0.
- Yin, Z.Y., Jin, Y.F., Shen, J.S., and Hicher, P.Y. 2018. Optimization techniques for identifying soil parameters in geotechnical engineering: Comparative study and enhancement. *International Journal for Numerical and Analytical Methods in Geomechanics*, **42**(1): 70–94. doi:10.1002/nag.2714.
- Yu, H.S. 1998. CASM: A unified state parameter model for clay and sand. *International Journal for Numerical and Analytical Methods in Geomechanics*, **22**(8): 621–653. doi:10.1002/(SICI)1096-9853(199808)22:8<621::AID-NAG937>3.0.CO;2-8.
- Yu, H.S. 2006. *Plasticity and geotechnics*. Springer Science & Business Media, New York, USA.
- Yu, H.S., Khong, C.D., Wang, J., and Zhang, G. 2005. Experimental evaluation and extension of a simple critical state model for sand. *Granular Matter*, **7**(4): 213–225. doi:10.1007/s10035-005-0209-y.
- Zhang, Z., and Cheng, X. 2017. A fully coupled THM model based on a non-equilibrium thermodynamic approach and its application. *International Journal for Numerical and Analytical Methods in Geomechanics*, **41**(4): 527–554. doi:10.1002/nag.2569.
- Zhou, C., and Ng, C.W.W. 2015. A thermomechanical model for saturated soil at small and large strains. *Canadian Geotechnical Journal*, **52**(8): 1101–1110. doi:10.1139/cgj-2014-0229.
- Zymnis, D.M., Whittle, A.J., and Germaine, J.T. 2018. Measurement of temperature-dependent bound water in clays. *Geotechnical Testing Journal*, **42**(1): 232–244. doi:10.1520/GJT20170012.

List of symbols

C	size of plastic potential surface	AQ14
e	void ratio	
f^{MY}, f^{TY}	mechanical and thermal yield limits	
g^{MY}	mechanical plastic potential	
k	XXXX	
M	slope of CSL in p - q space	
n	stress state coefficient	
$N_{(T)}$	specific volume on NCL at $p = 1$ kPa at temperature T	
OCR	overconsolidation ratio	
p, q	effective mean and deviatoric stress	
$p_{c(T)}$	preconsolidation pressure at temperature T	
$p_{c0(T_0)}$	initial preconsolidation pressure at T_0	
p_T	XXXX	
$p_{T(T)}$	effective stress at transition temperature	
$p_{x(T)}$	critical state stress at temperature T	
$r(T)$	spacing ratio at temperature $T (= p_{c(T)}/p_{x(T)})$	
T_0	room temperature	
v	soil specific volume ($= 1 + e$)	
α	drained elastic volumetric thermal expansion coefficient	
β, β_0	material parameter for thermal evolution of TY	
$\Gamma_{(T)}$	specific volume on CSL at $p = 1$ kPa at temperature T	
Δu	excess pore-water pressures	
δ_{ij}	Kronecker delta	
$\varepsilon_v, \varepsilon_d$	volumetric and deviatoric strains	
	principal strain components	
$\varepsilon_v^e, \varepsilon_d^e$	elastic volumetric strain and elastic deviatoric strain	
$\varepsilon_v^p, \varepsilon_d^p$	plastic volumetric strain and plastic deviatoric strain	AQ15
$\varepsilon_v^{mp}, \varepsilon_v^{tp}$	mechanical and thermal components of ε_v^p	
ε_d^{mp}	mechanical component of ε_d^p	
ζ	material parameter for thermal evolution of spacing ratio	
η	stress ratio ($= q/p$)	
θ	material parameter for thermal evolution of preconsolidation pressure	
κ	slope of swelling line in v - $\ln p$ space	
λ	slope of NCL in v - $\ln p$ space	
$d\lambda_m$	plastic multiplier	
μ	Poisson's ratio	
$\xi_{(T)}$	state parameter at temperature T	
$\xi_{R(T)}$	vertical distance between NCL and CSL	
σ_{ii}	XXXX	
σ_{ij}	principal effective stress tensor	
ω	material parameter controlling development of ε_v^{tp}	

AUTHOR QUERIES

Please answer all queries requiring corrections. Those left unanswered will be assumed to be correct.

AQ1: Please note that at the first list of the Introduction, the first item "Temperatue influences the NCL," the definition of NCL has been added. Following CGJ style, acronyms must be defined at their first use in the abstract and main text and solely the acronym is used thereafter. Changes have been made throughout.

AQ2: "Yu (1995)" is not in the reference list. Please add to the list or delete here.

AQ3: Can. Geotech. J. uses the standard mathematical typesetting conventions of single-letter scalar quantities in italics, vectors in bold italics, matrixes in bold upright, and tensors in sans serif bold italic. Please check carefully to see that we have properly typeset your mathematics.

AQ4: " $N_{(T)}$ and $\Gamma_{(T)}$ denote the specific volumes of the temperature-dependent NCL and CSL at $p = 1$ kPa, respectively" changed to " $\Gamma_{(T)}$ denotes the specific volume of the temperature-dependent CSL at $p = 1$ kPa" because eq. 2 does not contain the variable $N_{(T)}$ (it is only shown in Fig. 2). Please verify. **Yes, this is correct.**

AQ5: "Figure 4 shows. . ." changed to "Figure 5 shows. . ." to be consistent with the content of the figure. Please verify. **Yes, this is correct.**

AQ6: "The determination procedure and typical values of them were elaborated by Yu (1998)." has been changed to "The determination procedure and typical values of the parameters were elaborated by Yu (1998)." Is this correct? Please verify. **Yes, this is correct.**

AQ7: In Table 1, the magnitude of ω is $10^{-5}/^{\circ}\text{C}$. Please verify for consistency. **This should be -5 as given in Table 1.**

AQ8: "De Bruyn and Thimus 1996" is not in the reference list. Please add to the list or delete here. **Delete please.**

AQ9: At "and this leads to underestimation of peak strength for tests at OCR = 4 (Fig. 14c)." the figure number has been changed to "Fig.15c" because it would refer to Fig. 15c. Is this change correct? Please verify. **This is correct.**

AQ10: "in the plot of volumetric strain versus shear strain (e.g., Fig. 14c)" has been changed to "in the plot of volumetric strain versus shear strain (e. g., Fig. 15c)" because it would refer to Fig. 15c. Is this change correct? Please verify. **This is correct.**

- AQ11: "...are allowed to vary with temperature, which dependent on the combined hardening ..." has been changed to "...are allowed to vary with temperature, which are dependent on the combined hardening..." Please verify. **This is correct, thanks.**
- AQ12: "Bourne-Webb et al. 2009" is not cited in the manuscript. Please add an in-text callout or delete this reference. **Delete please.**
- AQ13: "Yao et al. 2009" is not cited in the manuscript. Please add an in-text callout or delete this reference. **Delete please.**
- AQ14: Following CGJ style, all variables that appear in the paper, figures, and tables must be in the List of symbols with their respective definitions. Conversely, variables in the List that are not used in the paper, figures or tables do not appear in the List. Please verify that all symbols and definitions that have been added are correct and provide the definitions where XXXXs appear. **It is verified.**
- AQ15: In the List of symbols, the symbol ε_d^p is given definition "elastic deviatoric strain". This has been changed to "plastic deviatoric strain". Is this change correct? **Yes, this is correct.**
- AQ16: At Fig. 8 caption, please provide a brief description of each figure part where XXXXs appear.
- AQ17: At Fig. 15 caption, please provide a brief description of each figure part where XXXXs appear.
-